UNIVERSITY OF OKLAHOMA

GRADUATE COLLEGE

An Experimental Setup to Measure Argon Leak Rate Through Barriers for Static and Rotational
Motion

A THESIS

SUBMITTED TO THE GRADUATE FACULTY

in partial fulfillment of the requirements for the

Degree of

MASTER OF SCIENCE

By

MILAD NAJAFBEYGI
Norman, Oklahoma
2022

An Experimental Setup to Measure Argon Leak Rate Through Barriers for Static and Rotational Motion

A THESIS APPROVED FOR THE
SCHOOL OF AEROSPACE AND MECHANICAL ENGINEERING

BY THE COMMITTEE CONSISTING OF

Dr. Zahed Siddique

Dr. Pejman Kazempoor

Dr. Iman Ghamarian

Acknowledgments

Table of Contents

List of Figures

List of Tables

ABSTRACT

As a greenhouse gas, methane significantly impacts global warming and air pollution. Oil and gas production, crude oil transportation, refining, and natural gas processing, transportation, and distribution are considered the main sources of methane emission in the oil and gas industry. Specifically, valves, joints, and moving parts where barriers were used have a magnificent role in methane emission. To address this problem, International Standard Organization(ISO) through ISO 15848 suggested that the oil and gas industry test the fugitive emission on their products with helium as a testing gas. Although, helium is an inert gas and its specifications make it an ideal gas for emission tests in the oil and gas industry, difficulty in production, transportation, high price, and global helium shortage lead us to find an alternative material. In this study, a setup was built to test argon emission in 25C, 121C, and 204C and pressure ranges of 600, 2250, 3750, 6750, and 10,000 psi on v-rings for static and rotational shafts with 2 rpm and 10 rpm. Experimental results were used to generate a machine learning model. Finally, a general polynomial formula was presented based on the machine learning model for static and rotational shafts with 2 rpm and 10 rpm. Results show the impact of temperature and rotational shaft's speed on leak rate is significant. This study's results apply to the valve, compressors, and any dynamic seal test process. Generally, the applications of this study can be to reduce the cost of the production and leak rate tests in rotational equipment design for the oil and gas industry.

Chapter One: Argon Emission

1.1 Introduction to Argon Emission

As a result of fugitive methane emissions from exploration and production endeavors and supply lines, the oil and gas industry has raised serious concerns regarding its contribution to greenhouse gases [1]. In particular, methane poses a severe threat to the atmosphere "due to its capacity to trap by volume 28 times more heat than carbon dioxide" [1]. "Emissions from valves account for 60% of the total methane emissions from a refinery, with as much as 80% of the leakage, per valve, occurring at the valve stem" [1]. For several years, fugitive methane emissions caused by valve leaks have been significant [1]. For industrial valves in the oil and gas industry, something must be done about emissions across barriers. It is only recently that organizations such as the Oil and Gas Climate Initiative (OGCI) and various governments around the globe have taken action [1].

Oil and gas operations are divided into three broad categories by the Intergovernmental Panel on Climate Change (IPCC) Guidelines:

  I.   Oil and gas production.

  II.   Crude oil transportation and refining.

 III.   Natural gas processing, transportation, and distribution.

All three types cause emissions. According to IPCC Guidelines for national greenhouse gas emission inventories, fugitive oil and gas operations emissions are non-combustion sources [2]. The IPCC Guidelines give the following definition of emissions: "Intentional or unintentional release of greenhouse gases may occur during the extraction, processing, and delivery of fossil fuels to the point of final use. These are known as emissions." (page 4.6) There are a number of

reasons that cause emissions to occur from oil and gas activities, including leaks from equipment, process venting, evaporation losses, and disposal of waste gas streams (such as venting or flaring), as well as accidents and equipment failures [2]. In addition to the equipment used, the design of the systems, maintenance, operating conditions, and other elements all play a critical role in determining the number of emissions. According to the requirements of different agencies, testing and qualification guidelines are available in relation to fugitive methane emissions, such as ISO 15848, TA-Luft, and API 622, 624, and 641 [3].

We have set out to characterize fugitive methane emissions from industrial valves to determine how they are classified in accordance with ISO 15848-1, which is the standard of the International Organization for Standardization (ISO). The term 'emission,' as used in this standard, is defined as a "chemical or mixture of chemicals, in any physical form, which represents an unanticipated or spurious leak from the equipment on an industrial site" [4]. As oil and gas industry-related emissions are unavoidable, it is imperative to understand how these emissions behave with that industry. The ISO 15848-1 standard describes leakage measurement procedures, leak rate classification schemes (tightness classifications), and qualification methods for emissions due to industrial valves that contain methane [4]. To categorize the valves' industrial applications, valve manufacturers use these classifications to organize the valves. Most manufacturers rarely use methane in their facilities to test such valves because of the cost of the gas and the possibility that it could cause an explosion under high pressure if it is used [5]. As a substitute for methane, helium is another gas that can be used to test industrial valves when methane is not an option. There are several reasons to use helium: being an inert gas, non-flammability in high pressure and temperature, and having a small molecular size, makes it a great testing gas for leakage tests. On the other hand, it is not easy to work with and store and is expensive compared to other gases [6].

With the ISO 15848-1 standard, there are specified leak rates for helium with different tightness classes and methane concentrations acceptable for each of the three tightness classes. There has been a shortage of helium in the market for several decades due to the difficulties associated with producing and storing helium.

The reason behind this study is the shortage of helium which makes it expensive; hence helium is no longer considered an ideal testing gas [7]. There is currently some discussion about the possibility of using alternate test gases for leak testing applications, and argon has so far been found to be a popular choice. [5]. This project focuses on argon emission across seals on valves stems from investigating if could use argon. To do this, it is necessary to: have a proper setup to run the tests and get the results to compare the emission between argon, helium, and methane. The very first part of this study is about building a setup that could handle the experiments in a range of temperatures and pressures for static and dynamic conditions since our focus here is on moving components of the oil and gas industry. As discussed above, these moving and rotational parts have a high contribution to emissions in the oil and gas industry. The results of this study are applicable to the valve, compressors, and any type of dynamic seal test process. Generally, the applications of this study can be to reduce the cost of the production and leak rate tests in rotational equipment design for the oil and gas industry.

1.2 Helium Leak Testing

Helium as a testing gas helps manufacturers identify unwanted leaks in the manufacturing processes of valves and components with barriers and seals [6]. In addition to porosity, minor welding defects, microcracks, faulty seals, incorrect component assembly, etc., several other factors can lead to an unforeseen leak. In the context of emissions testing, ISO 15848-1 outlines a

specific measuring process for testing valve leakages [4]. This method involves a pressure change caused by helium accumulation and has applied the same approach to measure the leak rate with argon.

1.3 Why Use Helium or Argon

Helium is one of the most widely used test gases due to its small molecule size and inert nature [6]. In addition to being inert, non-explosive, non-toxic, non-reactive, and do not contribute to greenhouse gas emissions, helium and argon can be safely discharged into the atmosphere [8]. These inert gases exist in the atmosphere but are considered trace and extremely rare. Hence, "there is little ambient 'noise' to interfere with leak measurement" processes [8]. Since the mass spectrometers can detect both gases, it is possible to track helium and argon leakages with the same device [6]. However, it is easier to collect and keep argon samples than helium because argon molecules are more prominent and easier to save in a sampling container. In mass spectrometer machines, there is equipment to recapture the helium from the atmosphere, but helium is extremely difficult to recapture, and it is difficult to store. In addition, argon is more affordable than helium as a testing gas. It is easy to produce, transport, and keep. Hence, argon is an even more attractive candidate for being a primary testing gas.

1.4 Global Helium Shortage

It is becoming an increasingly scarce resource because helium is widely used across industries such as oil and gas, space technology, and medical instrumentation. Since it is free to float around the atmosphere, it is already challenging to capture. There are running out of helium reserves discovered by oil companies, and scientists struggle to find new sources. Helium has been in short supply for the last few years, and there is little hope of increasing its supply in the near future [9].

Since helium is not a renewable resource, finding a solution is necessary if it remains a primary resource for research and manufacturing. In order to find a realistic solution, one must look for alternatives to helium that can be used for the application.

1.5 Problem Statement

The objective of this study is to analyze argon leak rate in static, 2rpm, 10 rpm, and at room temperature, 121C and 204C to get a leak rate and be able to have a general model for argon leak rate so can find an equivalent for methane leak rate in rotational shafts. As predictive machine learning methods, an Artificial Neural Network, K-nearest neighbor, and support vector machine was used based on the complexity and nature of the data. In this study, an experimental setup was built to achieve the results. The setup contains a vessel with a symmetric configuration of barriers and the ability to collect the accumulated gas pressure on the low-pressure side. This setup can boost the test gas up to 10,000 psi and hold the pressure. In order to ensure consistency, each test has been repeated at least three times. After each set of experiments, the seals were tested. For these sets of tests, the rotational angle was +90 and -90 for 2 rpm and 10 rpm to resemble a motion in a valve, respectively, when it is in use and when it is abused.

1.6 Summary of Chapter One

This chapter discussed the importance of methane emission in the oil and gas industry and its global impact as an air pollutant. ISO suggested a standard for allowable leaks in products to address this problem. In ISO standard, helium has been introduced as a test agent. ISO recommended helium because it is an inert gas and easy to identify. Also, oil and gas product producers can safely do high-pressure and high-temperature tests with this gas on their products.

According to research in 2013, the world faces a severe shortage of helium and needs to find an alternative gas for emission tests in the oil and gas industry. In addition, the world needs helium for sectors such as health that directly impact humanity. This study suggests using argon instead of helium and developing a test setup to test the emission on argon for v-rings in multiple temperatures and pressures.

Chapter Two: ISO Standards

2.1 ISO 15848-1 Standard

A non-governmental organization responsible for creating national standards is the International Organization for Standardization (ISO) [4]. The ISO gives world-class specifications to ensure the quality, safety, and efficiency of products and systems. ISO 15848-1 is the focus of this report. According to ISO 15848, "the objective of this part is to classify the performance of various valve constructions and designs to reduce emissions" [4]. The gas will be applied at temperature when under pressure while being flammable or inert. For the tests to be successful, the fluid had to contain 97% purity of helium gas and 97% purity of methane [4]. As a result of differences in operating conditions and dangers during industrial use, the criteria for each class differ. Due to these varying conditions, greater or lesser valve performance will result; therefore, the classes will indicate the appropriate minimum leak rates for three additional helium and methane conditions. Based on this standard, in this set of experiments, argon with 97% purity has been used.

2.2 Temperature Classes

The target temperature class in this set of experiments has been selected from Table 2-1 [4]. When the test is conducted at a different temperature than that specified in Table 2-1, the next lower class is applied in cases where the test temperature is above zero, or the next higher class in cases where the test temperature is below zero. [4].

Table 2-1:temperature classes [4]

(t-196 °C)	(t-46 °C)	(tRT)	(t200 °C)	(t400 °C)
−196 °C	-46 °C	Room Temperature	200 °C	400 °C

In this set of studies, room temperature, 204 °C, and 121 °C have been considered as test temperatures [4].

2.3 Total Leak Rate Measurement

Based on ISO15848-1, the leak rate can be measured as follow:

- Vacuum method (helium only): The leakage source is enclosed in a tight chamber, which is evacuated and then connected to the helium mass spectrometer.

- Bagging method (helium only): Two methods can be used to measure the leak rate of the stem sealing system by bagging:

  — The accumulation method is used in this study. In this method, the accumulated pressure of the test gas is measured by a pressure transducer.

  — The "Suck Through Method" is described as "the leakage source enclosed by a bagged volume. This volume, or bag, is connected to a helium mass spectrometer through a constant flow rate detector probe (sniffer). The extracted volume is replenished through a balancing tube with a length at least 50 times the probe inside diameter, connected to the atmosphere. Air passes through the bag, where it mixes with the leakage stream of the test gas. Then, it passes down the sniffer probe to the instrument detector. All leaked test gas passes through the helium mass spectrometer" (page 25) [4].

This study used the accumulation method to measure the argon leak rate as a test fluid.

2.4 Why Argon Has Been Used

Argon was discovered as the first noble gas. Sir Henry Cavendish first observed it in 1785. The noble gas argon is an excellent test gas since it is non-explosive, inert, and non-toxic. In addition, argon does not contribute to greenhouse gases, making it an attractive choice for leak detection testing. Moreover, it can be released into the atmosphere without causing any harm to the environment. The compound belongs to group 18 of the periodic table. Argon ranks third among Erath's most abundant gases. Approximately 0.934% (9340 ppmv) of the atmosphere consists of argon. There are two times as many argon molecules as water molecules. There is 0.0015% of argon in Earth's crust, making it the most abundant noble gas. Argon is a noble gas that is the most economical alternative to nitrogen when it is not a preferred gas. It is less thermally conductive. The gas is also environmentally friendly. With a melting point of -189.34 degrees Celsius, argon is an ideal candidate for testing applications that require sub-zero temperatures [10].

2.5 Summary of Chapter Two

Chapter two discussed the ISO standard for helium leak rate and classified it into three classes based on the leak rate. Here can see the temperature and pressure classes suggested by ISO. Also, in this chapter, the leak rate measurement methods are presented by ISO. By using the accumulated pressure, the leak rate is measured in this study. By the end of the chapter, argon has been suggested as a good alternative for helium, considering it is easy to identify, take the sample, store, and produce. All these attributes make argon an ideal alternative for helium. Also, argon is an inert gas, and approximately 0.93% of the atmosphere includes it.

Chapter Three: Test Setup And Its Components
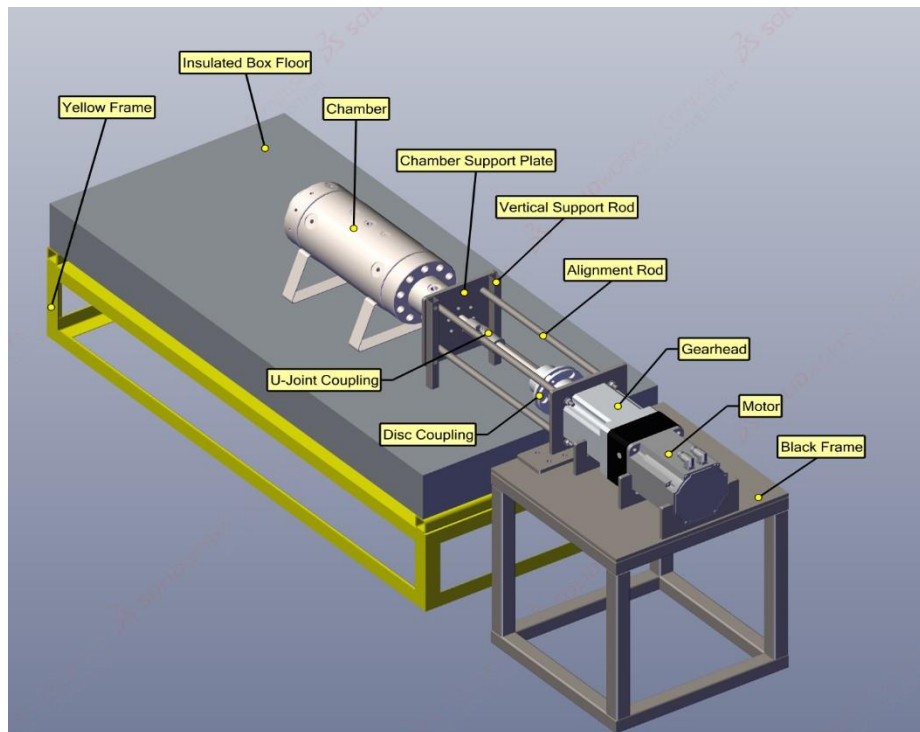
Figure 3-1: Complete assembly

3.1 Overview of the Test Setup

A metal test chamber has been used as a test vessel for experiments. The test vessel is a symmetric system that contains a high-pressure inlet valve in the middle and a low-pressure outlet valve on both sides of the vessel. Based on the pressure for each test, can either bost the argon into the chamber up to 10,000 psi or use bottle pressure. In order to measure the leakage from seals on the low-pressure side, the accumulated gas is measured. Two separate transducers for each side have been installed on the low-pressure side. For safety, both caps have been used on low-pressure sides. These safety valves can react when the low-pressure side has an accumulated pressure higher than 100 psi.

For monitoring the temperature, j-type thermocouples have been used. The thermocouples have been placed on the vessel exactly where have seals. Environmental temperature is monitored with separate j-type thermocouples.

For increasing the temperature, heating bands have been used. Four heating bands have been installed on the body of the vessel. These bands are controlled by a PID controller with a solid-state relay. In this set of experiments, the temperature is 121C, 204C, and room temperature, and have used argon as the test gas. A Labview program has been used to control all the system components, including the motor driver, heater bands, inlet and vent of the high-pressure and low-pressure gas, booster, and monitoring pressure in high-pressure and low-pressure parts of the system, and recording data. Figure 3-1 shows complete assembly. The followings are explanations of the different components have used in the test setup:

3.2 Overview of V-rings

Figure 3-2: A sample of homogeneous rubber v-ring [11].

Figure 3-2 shows a homogeneous rubber v-ring. The v-rings serve as lip seals or flinger rings. They are utilized to seal against dust, soil, grease, oil, or water splashes from the exterior. The v-ring turns with the shaft, fixing axially against the counter surface. V-rings are utilized in combination with other seals, like spiral shaft seals, but as a pre-sealing component for orientation.

V-rings are accessible and provide high adaptability in utilization for pressure-less operations. V-rings' typical applications are rolling mills, cultivating apparatus, and electric engines. Generally, v-rings are made from rubber or graphite, ad usually, they are mounted on shafts and seal the counter surface. A v-ring is usually designed to be slightly tighter than the shaft's outer diameter so it can clamp to the shaft. In v-rings, centrifugal forces act on the barrier lips when the rotational speed increases and reduces contact pressure. Due to this effect, v-rings at higher rotational speeds at very low friction losses are used [11].
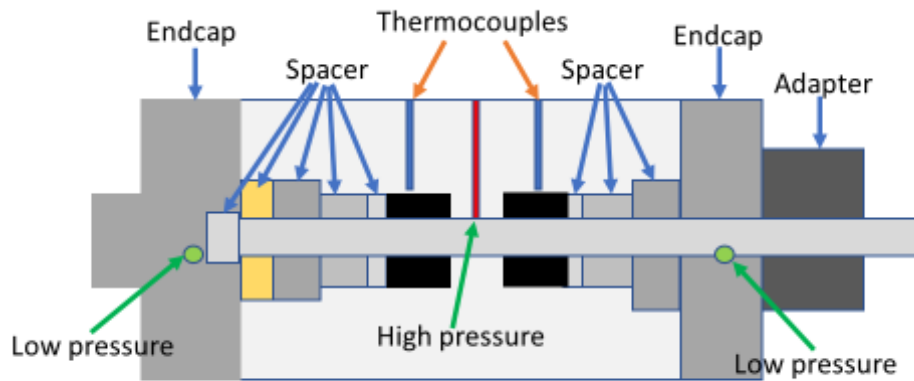
Figure 3-3: Test vessel.

This study used a symmetric test chamber to measure the leak rate at different pressures, temperatures, and rotational speeds in v-rings. The test setup contains multiple components, including temperature measurement systems, pressure control systems, pressure control systems, rotation control, power systems, and safety systems. Figure 3-3 shows a schematic of the test vessel.

Figure 3-3 shows different parts of the test vessel. This vessel is a symmetric system and contains two low-pressure zones on the sides and one high-pressure zone in the middle of the vessel. Since

the system is symmetric, it can install two sets of seals simultaneously in the middle of the vessel, and these seals are supporting meet three layers of spacers. The length of the first layer of spacers can be a variant base on the length of the barriers used in the test setup. In this setup, a central shaft passes through all the spacers except the last one in the end cap of the system. Two holes have been drilled in the top of the vessel for the purpose of measuring the system's temperature. These holes are going up to a very close distance to the seals. By instaInstallingouples inside these two temperature measurement holes can measure and record the temperature of the seals every second. In Figure 3-3, a yellow color spacer is shown. This spacer centralizes the shaft and provides smooth rotation for the shaft. There are two end caps in this system, and on the sides of each of these end caps. The end caps on each side of the vessel are installed with ten bolts. The end cap at the end of the vessel, shown on the left-hand side of the schematic in Figure 3-3, is a close endcap, and the end cap on the right-hand side is an open one that can pass the shaft through it. In this system, after installation, is:

- Pressurized with argon gas at 600, 2250, 3750, 6000, and 10,000 psi

- For room temperature, 121 degrees C and 204 degrees C

- With a static shaft and rotational shaft with 2 rpm and 10 rpm

For all these conditions, the accumulative pressure on both sides of the seals. It is designed with a double-face o-ring in order to prevent leakage from the open side of the endcap, and a cap closing component is installed on the head side of the vessel. This component has been used as a connection for the adapter plate. The adaptor plate is an aluminum plate that is installed on the head of the vessel and helps to have a better alignment with the electric motor components. The adaptor plate is connected to the motor through stainless steel rods.

13

3.3 Temperature Control System

3.3.1 Thermocouples

The system has been equipped with a set of thermocouples to check and control the environmental temperature and the temperature of the experimental setup. A j-type thermocouple was used in the setup to measure the temperature accurately. Considering the following descriptions j-type thermocouple has been selected:

The type j thermocouples are commonly used in industrial applications. There are some similarities between j-type and k-type, but the main difference is that j- type has a smaller temperature range and shorter lifespan than k-type. The j-type thermocouples can work on temperature ranges from -346 to 1,400F (-210 to 760C). When using direct thermocouple grade wire and 32 to 392F (0 to
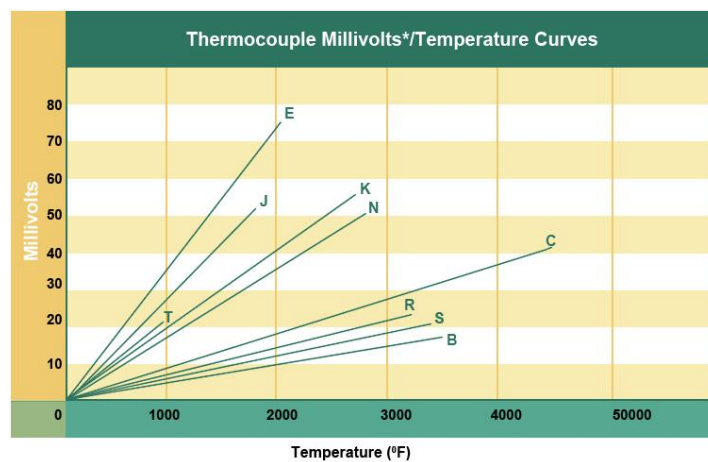
Figure 3-4: Millivolt/temperature diagram [12]

200C) for the extension wire. The standard error is +/- 2.2C or +/- 0.75% in j-type thermocouples [12].

14

J-type thermocouple grade wire and extension grade wire. These thermocouples are iron/Constantan and well suited to oxidizing atmospheres. In this setup, two thermocouples are used to read the temperature of the seals on each side of the vessel, and one thermocouple is used to measure the temperature of the environment [12].

Figure 3-4 indicates that j-type thermocouples can support up to 1400 F with more than a 50 millivolt voltage difference between 0 F and 1400F. The significant voltage difference shows how accurate is the thermocouple system [12].

3.3.2   Electronic Temperature Controller

As its name suggests, an electronic temperature controller is an instrument that controls temperatures without human intervention. The controller uses an input temperature sensor in a temperature control system, such as a thermocouple or a resistance thermometer, and compares the actual temperature with the setpoint temperature. A control element will then receive an output signal [13]. An example would be if a controller received temperature information from a sensor and sent it to a control device such as an electrical heater. It is important to remember that controllers are often only one part of a temperature control system, so the entire system should be analyzed and considered before choosing a controller [13].

3.3.2.1   On/Off Temperature Controller

On-off temperature controllers are the most basic control devices. There is no in-between condition for the output of this device. An on-off controller switch will only turn on when the temperature exceeds the setpoint [13]. When it comes to heating control, the result is on when the temperature is below the setpoint and off when it is over the setpoint. In this, a proportional–integral–derivative

controller (PID controller) is used, and to have a faster reaction, it has been connected to a solid-state relay.

3.3.2.2 Proportional Integral Control

An on/off control cycle is eliminated with proportional controls. The average power provided to the heater is reduced as the temperature nears a setpoint by a proportional controller. [13].

Figure 3-5: A typical PID controller[13]

Figure 3-5 shows a typical PID controller. Usually, can set a temperature by pressing the set and going to the program, and then putting a temperature in this controller. You rarely set a temperature, and the controller can stay on that temperature. So, here suggested having some experimental tests and considering the thickness of the material and the distance of the temperature measuring prob of the controller to the seals, consider some overshoot on the temperature.

3.4 Motor and Moving Parts

In this set of experiments, a Kollmorgen AKM7 series synchronous servo motor was used to provide a dynamic rotational motion. To make sure that the motor has enough power to rotate the

shaft with a constant speed in any condition following specifications have been considered in choosing the motor:

- It delivers approximately 100 ft-lbs of maximum torque

- It has a continuous stall torque of about 40 lb-in.

- The maximum rotation speed of this motor is 3500 rpm

- The motor needs a 240 volt AC supply power.

A typical servo motor used in this setup is shown in Figure 3-6.

Figure 3-6: A typical servo motor

3.4.1 Gearhead

Kollmorgen suggests the gearhead selection for the AKM7 synchronous servo motor. Kollmorgen presented a planetary design known to be durable and better for higher torque applications due to the increased number of gear teeth and surface contact. Also, a better surface contact can

effectively reduce noise and enhance stability. These gearheads are customizable to any gear ratio, precise, and produce a minimal backlash.

The gear ratio of 28:1 has been used for this system, which produces a peak torque of about 2800 ft-lbs and a continuous stall torque of about 1050 ft-lbs. A visual representation of the gearhead is shown in Figure 3-7.

Figure 3-7: A typical gearhead

3.4.2 Motor Controller

To control the motor, and AKD motor driver has been used. The motor driver can perform a -90 and +90 degree motion with multiple speed options. In this set of experiments, the shaft rotates between -90 and +90 degrees at 2 rpm and 10 rpm.

3.4.3 Shaft Alignment

One of the most crucial aspects of this project is ensuring that the shaft does not exhibit any parallel or angular misalignment relative to the opening inside the vessel. Any parallel misalignment more significant than one-thousandth of an inch can cause numerous unforeseen problems. The main issue that this misalignment can cause is irreversible damage to the shaft and seals. The biggest issue stemming from the shaft misalignment is that if the surface of the shaft is scratched, a new one will have to be machined, which could come with a lead time of one week or longer. Misalignment can cost a great deal of time and money. Figure 3-8 is a side view of the vessel, shaft, and couplings.
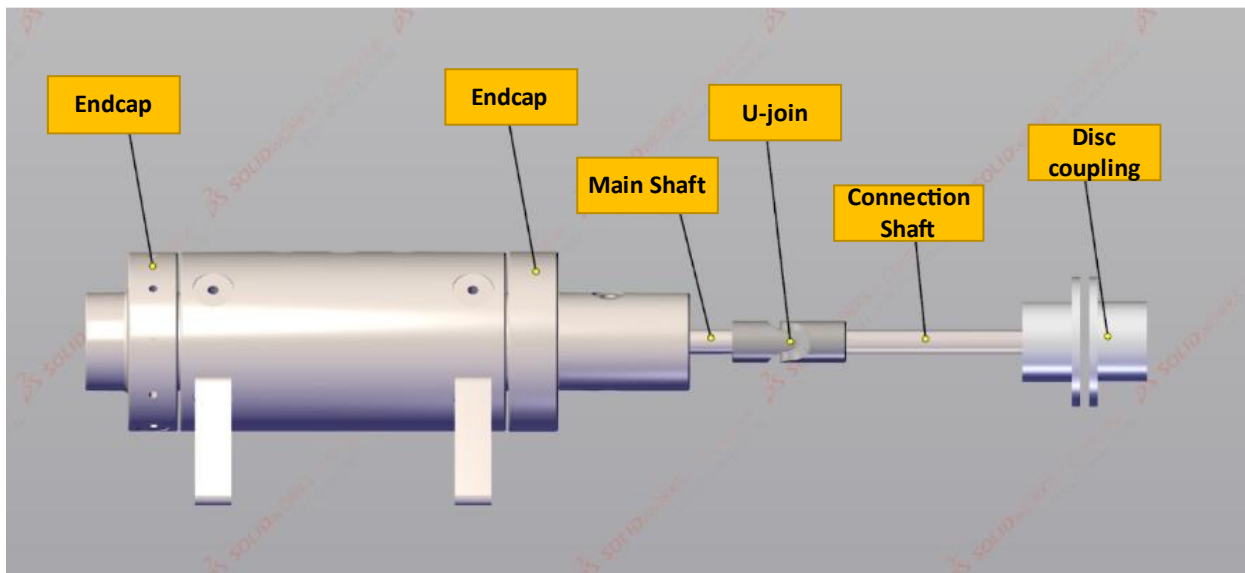

Figure 3-8: Side view of vessel, shaft, disc, and u-joint coupling

The u-joint coupling in the middle of the shaft can significantly reduce the possible alignment errors that could have occurred. This coupling goes inside the cooling box and joins the shaft to an extension shaft. This coupling allows for easier alignment because it corrects any angular

misalignment presented from the extension shaft. The shorter length of the shaft almost guarantees that no damage will occur to the shaft or seal contained within the vessel. Here the u-joint has 10-degree flexibility. A disc adaptor has been used to connect the gearhead to the extension shaft. A set of alignment rods has been used to fix all the structures. An aluminum adaptor plate has been connected to the vessel's head to connect the motor through the alignment rod motor.

3.4.4   DAQ Device

The data acquisition control device (DAQ) USB-6353 from National Instruments was utilized for this study. Considering the number of devices that need to connect to the DAQ and the data recording speed, a (DAQ) USB-6353 has been used. The followings are some of the specifications of this device:

This device can accommodate 16 differential channels or 32 single-ended channels. Ideally, 16 differential channels can be operated from a single-ended channel of 32. A notable characteristic of the USB-6353 DAQ device is its high sampling rate [14]. This sampling rate for a single channel is1.25 MS/s and for multiple channels are, 1.00 MS/s. For this device, the timing resolution of the input channels is 10 ns. Also, the timing accuracy in USB-6353 NI is 50 ppm [14].

It is possible to trigger this device with the help of a single analog trigger, which can be used for various purposes. The source level of the trigger for AI<0.31> is the ±Full scale. In addition, the source level of the catalyst for APFI<0.1> is ±10 Volts. It is possible to measure the signal with a resolution of 16 bits with analog triggers. These analog triggers can also be switched between multiple modes. For example, analog edge triggering is the most commonly used method for analog triggers. The input resistance of an analog trigger is 10 k Ohm. Multifunction input/output devices of the USB-6353 NI have different protection values for the 'on' and 'off' modes of the

device. The protection voltage is ±30 V when the power is on and ±15 V when the power is off [14].

A total of four analog output channels are available in this device, with a 16-bit resolution. As well as analog output channels, these units can also take in digital signal inputs. These channels provide Output Resistance, and it is equal to 0.2Ω. Also, the current for the output of this device is ±5 mA. Figure 3-9 shows the NI USB-6353 DAQ device with its connection terminal. It has been performed here that the analog connection has been made directly between relays and DAQ by using a direct connection. A signal conditioner is connected to the thermocouples, and the thermocouples are directly connected to the DAQ [14].
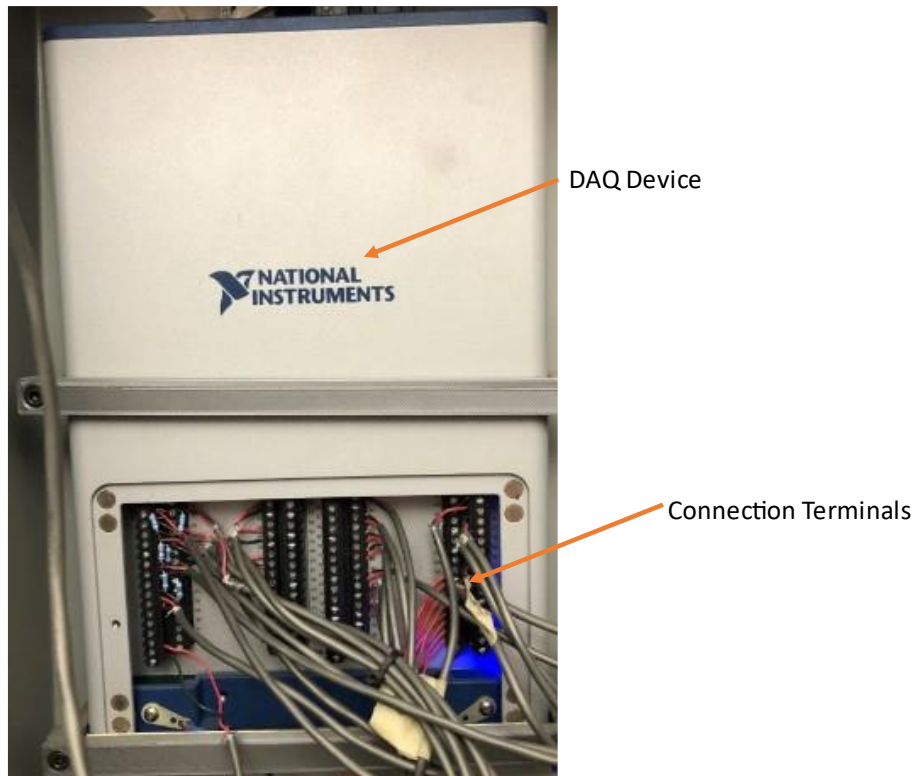
Figure 3-9: NI USB-63-53 DAQ

3.4.5 Booster

A two-stage triole airhead gas MAXmotor booster has been used in this setup. It is an alternative to high-pressure stationary compressors. These boosters do not need electrical power or lubrication and provide a compact, lightweight design. Therefore they provide a more flexible source for delivering high-pressure gas [14].
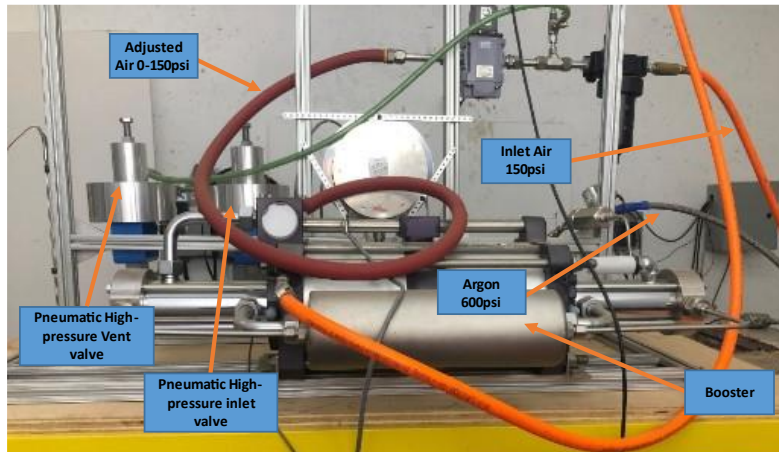
Figure 3-10: Gas pressure booster

Figure 3-10 shows the pressure booster. The booster in the setup has been connected to a 150 psi pressured air tank as a power supply and is controlled through an electronic regulator and the DAQ device. The following schematic in Figure 3-11 shows the high-pressure airflow used to generate power for the booster.
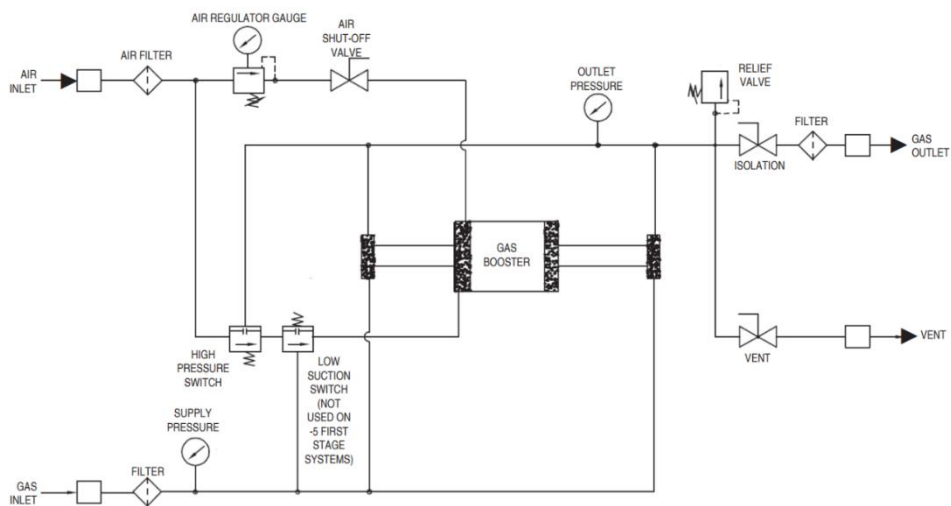
Figure 3-11: Booster assembly

To run the booster, you need 150 psi air power. The air passes through an air filter and is regulated by an electronic regulator shown in Figure 3-12. In this set of experiments, the test gas is argon; the test gas is an enterenterse booster from a separate inlet. Desire pressure in the outlet is controllable with an electronic regulator controlling with DAQ [15].
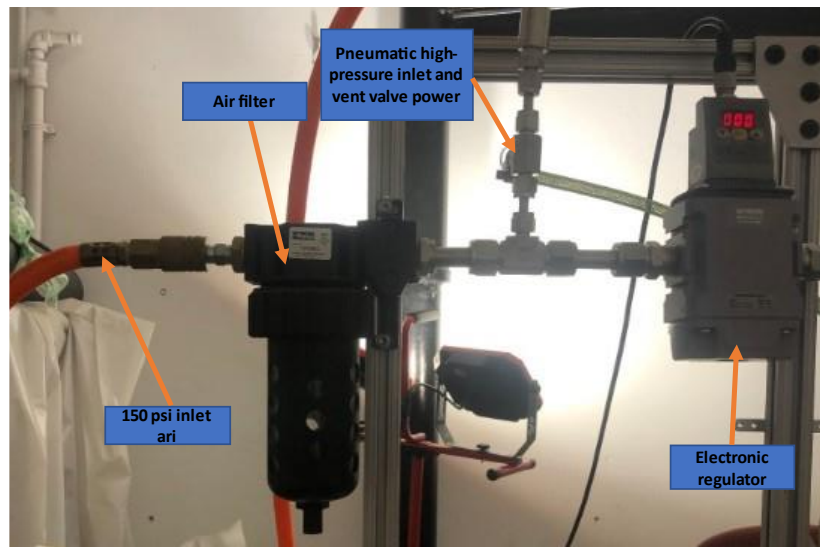
Figure 3-12: Electronic regulator and air filter

3.4.6 Safety

For safety, this setup has been assembled in a bunker, and all the components can be controlled by a DAQ connected to a computer program. The high-pressure inlet and outlet valves are powered with high-pressure air (150 psi) in the setup. A manually adjustable high-pressure valve has been attached to the high-pressure air-powered valve to prevent damage to barriers during depressurization of the high-pressure side.
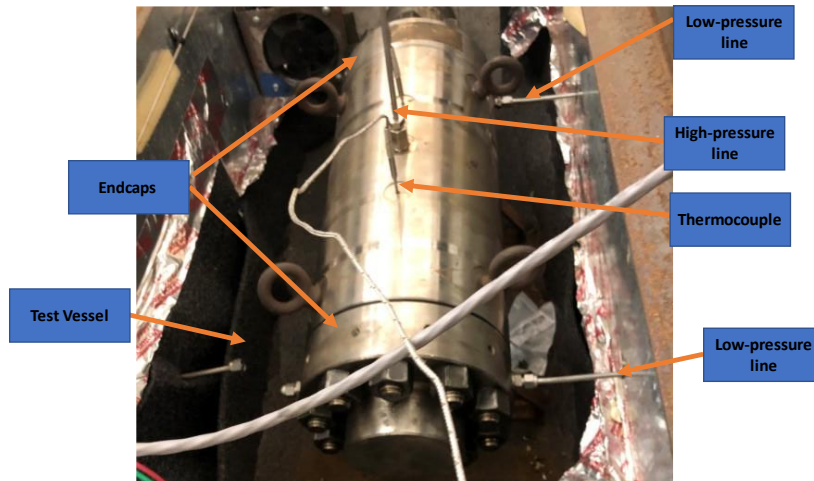
Figure 3-13: Test vessel and its connections

The test vessel has an endcap on each side. Each endcap is fixed to the vessel's main body with 10 bolts. The shaft is connected to the U-joint from one side, and the other side has been fixed and entirely closed by an endcap This fixture blocks the shaft from one side and does not let the shaft shoot out in high-pressure experiments. The other side of the shaft has been constrained by a gearhead and motor, a heavy structure that will stop the shaft from moving forward.
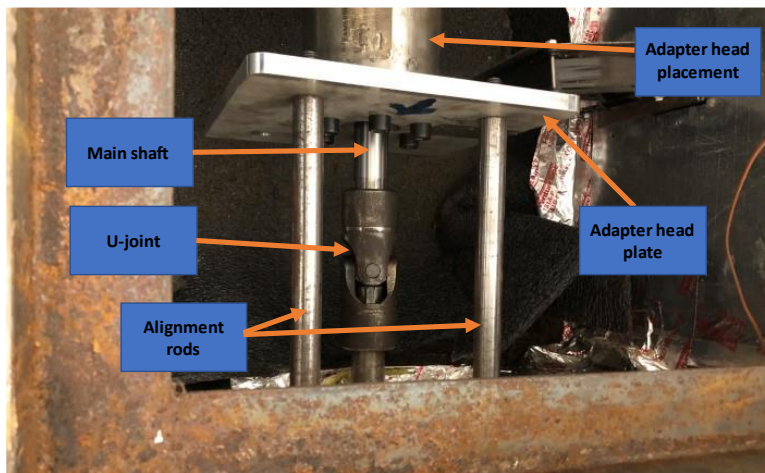
Figure 3-14: Test vessel front components

Figure 3-14 shows the front components. To keep the moving parts aligned with the vessel, an aluminum plate has been installed on the head component of the test vessel. The aluminum plate also works as an adaptor to connect the alignment rods to the test vessel. As it is shown in Figure 3-14, a u-joint connects the shaft to the motion transformer connector. So, the u-joint can provide up to 10-degree tolerance in miss alignment.
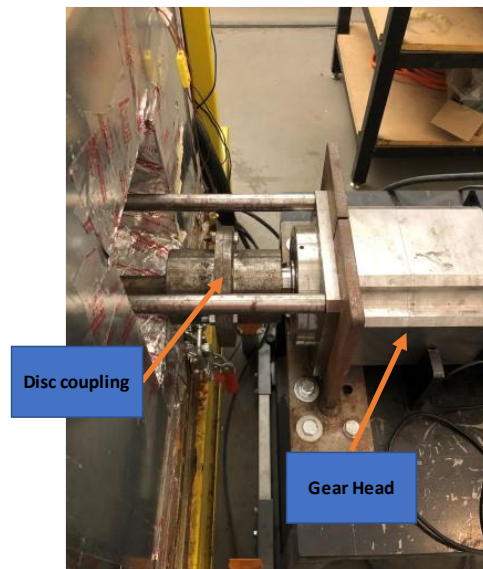
Figure 3-15: Gearhead front fixture

As shown in Figure 3-15, the gearhead has been fixed to the table with three bolts and two L-shaped parts. The alignment rods from the other end are connected to the gearhead and make a fixed structure between the motor, gearhead, and vessel.

3.4.7 High-Pressure Line

A two-stage valve system has been used to increase the safety of high-pressure lines. In this system, after increasing pressure on the high-pressure side, a valve closes and traps the high-pressure gas inside the vessel. Using this system, the high-pressure side can be depressurized and have much more safety during high-pressure experiments.

The vessel is a symmetric system on the low-pressure side, so there are two exits for low-pressure gas. The low-pressure side fixture is shown in Figure 3-16.
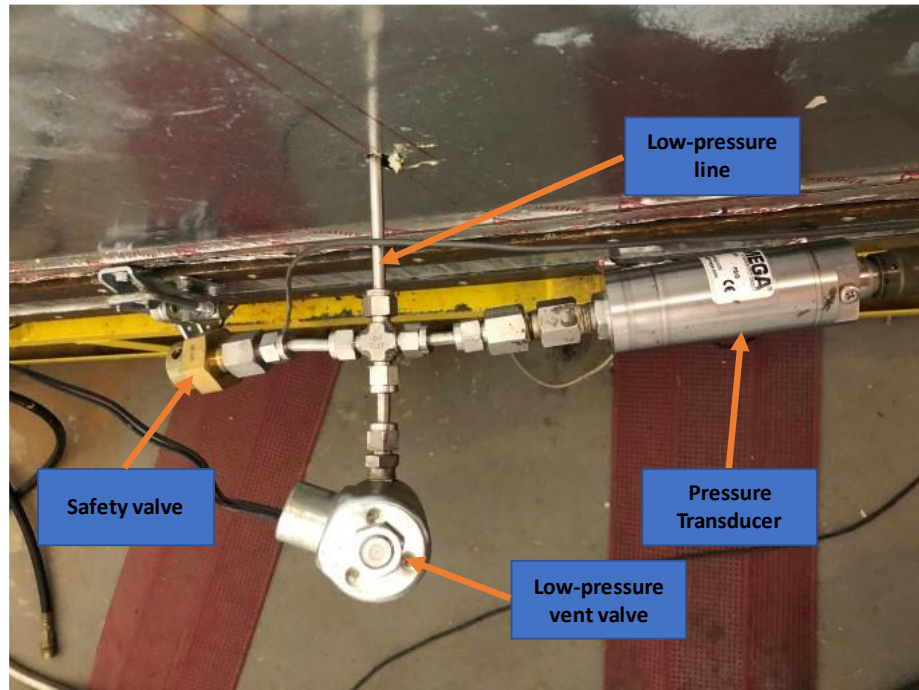
Figure 3-16: Low-pressure side fixture

Figure 3-16 shows the low-pressure side has three components. These three components include a pressure transducer to read the pressure on the low-pressure side powered by a 24-volt power supply and connected to a DAQ device. This pressure transducer can hole up to 150 psi. A low-pressure electronic valve is connected to the DAQ device and programmed to automatically open when the gas pressure exceeds 15 psi. Figure 3-17 shows the last safety part of the low-pressure side, which is a mechanical safety valve.
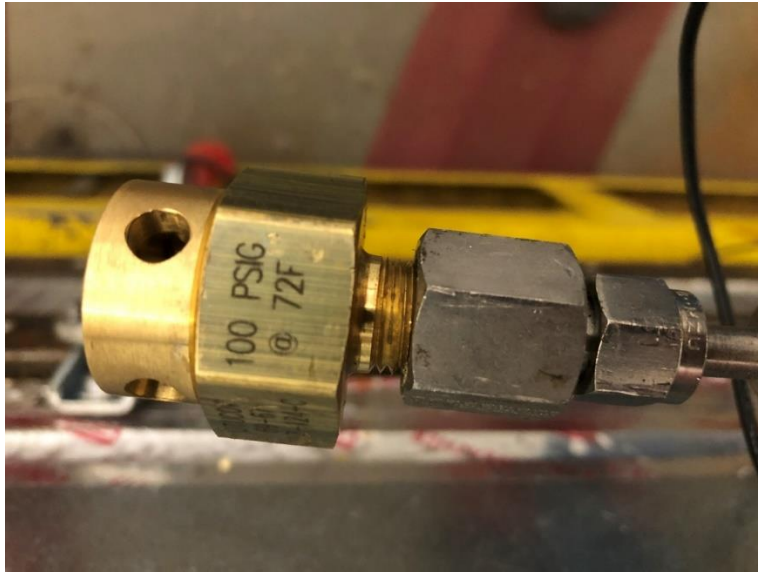
Figure 3-17: Mechanical safety valve

This valve can hole up to 100 psi at 72 Fahrenheit. The valve has a thin layer of material inside, exploding when the pressure exceeds 100 psi.

Since the test media is a gas, two Oxigen sensors have been installed in the experiment and control rooms. This sensor measures Oxygen levels in the room and has been equipped with an internal alarm system. Figure 3-18 shows the Oxigen sensor mounted in the experiment room.

Figure 3-18: Oxigen sensor

The Oxygen sensors have a separate power supply connected to an external alarm system and an exhaust fan for safety. Figure 3-19 shows the individual power supply for Oxygen sensors and alarm systems.
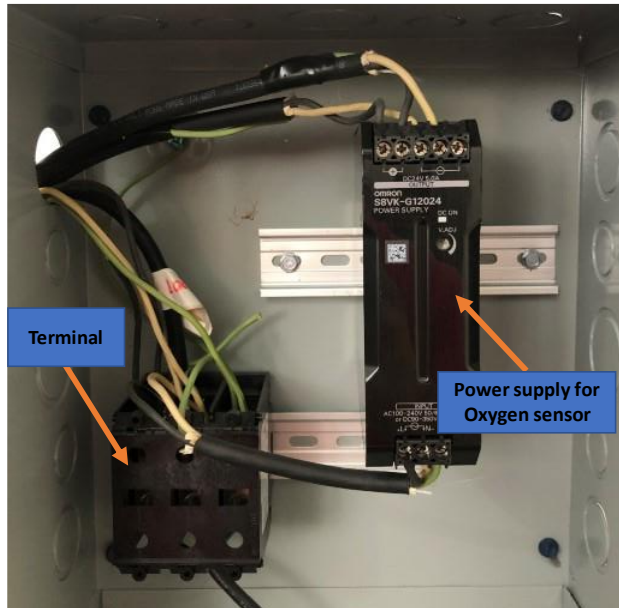
Figure 3-19: Individual power supply for Oxygen sensors and alarm systems

In Figure 3-19, a 24 volt supply power has been used to provide power for the Oxygen sensor and its alarm system. This power supply has been secured in a separate box from the setup. This power supply provides power for a visual and voice alarm.

3.5 Summary of Chapter Three

This chapter has an overview of the system. Here mentioned, the system has a pressure range between 600 to 10,000 psi and a temperature range of room temperature to 204C. The system has thermocouples and a PID controller to read, record, and control the heating bands to operate in

various temperatures. Furthermore, the test vessel has a symmetric configuration of seals. Also, the system can run static and dynamic tests with this system. The motion control system is programable and used to run experiments on 2rpm and 10 rpm in addition to static tests. To control the system, convert data to workable data for the computer, and record the data, a DAQ device has been used. Finally, safety valves and Oxygen sensors with separate power supply have been used to satisfy the safety factors.

Chapter Four: Test Running Process

This chapter has an overview of the installation and operating procedure of the system. Also, different components of the existing system have been shown.

4.1 Experimental Procedure Flowchart
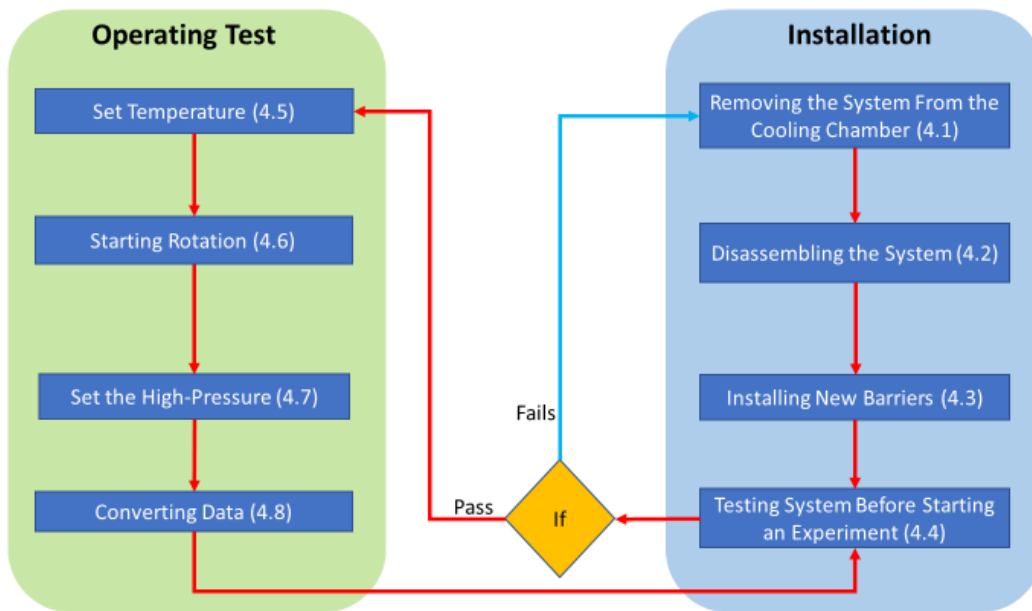
Figure 4-1: Experimental Procedure Flowchart

Figure 4-1 shows the experimental procedure and actions that need to be taken wheninterruptiontion happens. The flowchart includes operational and installation parts. As part of the installation process, the system is removed from the cooling chamber, disassembled, new seals are installed, and the system is tested. So, if the seals could not pass the initial test, the installation needs to be reviewed, and a new set of seals might be required. If the seals can pass the initial test, the operational portion starts. In the operational part, first, the temperature is adjusted based on static or dynamic tests, the shaft rotational speed adjis usted, and the high-

pressure gas is introduced on the high-pressure side. Finally, the recorded data is converted to be analyzed.

4.2 Removing the System From the Cooling Chamber

The very first part of a test running process is seal installation. Take the vessel out of the box to install the seals. The first stage is disconnecting the vessel from the motor. As shown in Figure 4-2, the motor has been connected to the vessel by two alignment rods.

So open the alignment rods from the end connected to the vessel adapter head. Then Free the
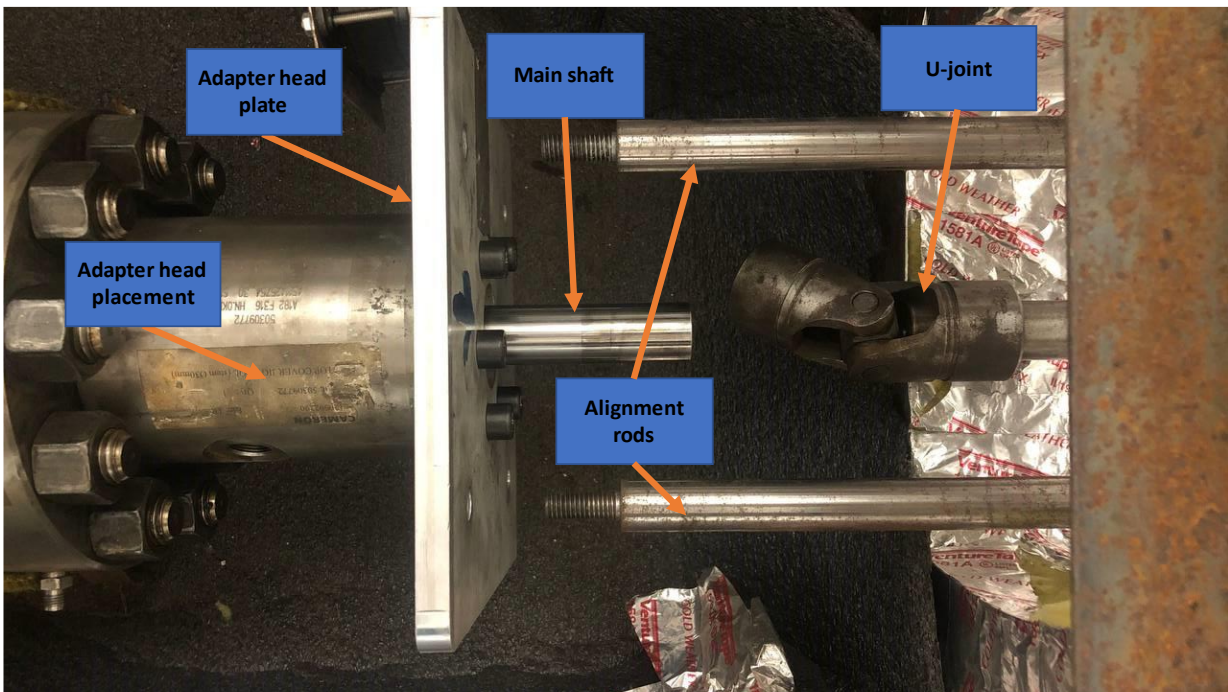
Figure 4-2: Opening the alignment rods and u-joint

vessel's shaft by pulling backward the motor system. In this stage, the connection between the motor connector shaft and the vessel's shaft will be open from the point that a u-joint has been inistallinstalledint link is fixed between the main shaft and the connector shaft of the motor by using mechanical keys on both sides.

Free the main shaft from the motor. Open the high-pressure line connection from the top of the vessel and its connection to the high-pressure inlet valve shown in Figure 4-3.
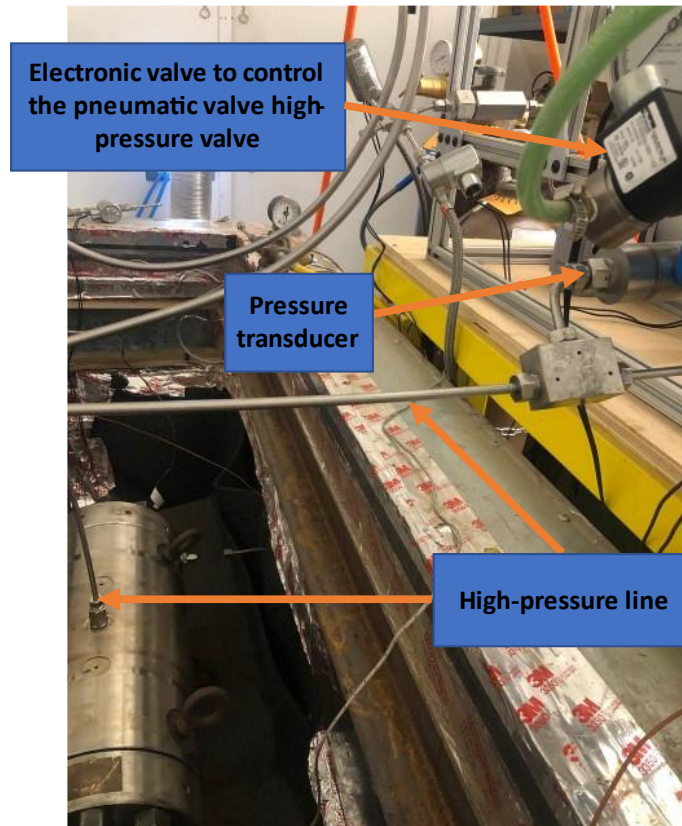
Figure 4-3: High-pressure line

Before opening any low-pressure or high-pressure connections, run the LabView program and ensure that the system has been completely depressurized. Any pressure in both low-pressure or high-pressure sides will make opening the fittings very difficult or damage them. After opening the high-pressure fittings, open the low-pressure fittings and disconnect the electronic valves. Figure 4-4 shows the low-pressure fittings.
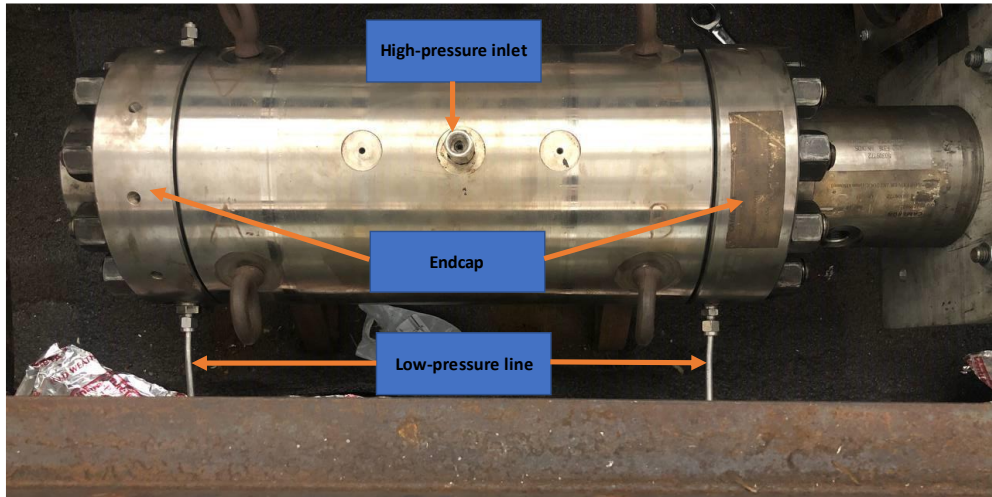
Figure 4-4: Low-pressure lines

Must take it out of the cooling chamber to open the vessel. In the setup, use a pulley system to take

the vessel out and place it on a steel table to start the disassembly process (Figure 4-5).

Figure 4-5: Pulley system

4.3 Disassembling the System

To disassemble the setup, open the adapter plate on the front of the vessel. Six bolts have fixed this adapter plate (Figure 4-6).
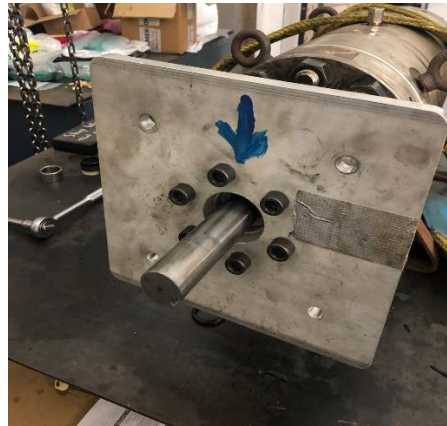
Figure 4-6: Adapter plate direction

Then the head of the vessel that holds the adapter plate needs to be opened, shown in Figure 4-7 as part A. On the other side of part A, connected to the endcap, two o-rings are installed to prevent the leak from the low-pressure side to the environment.

Figure 4-7: Adapter head connection

Next, open the ten nuts of the two endcaps of the vessel with an impact wrench (Figure 4-8).
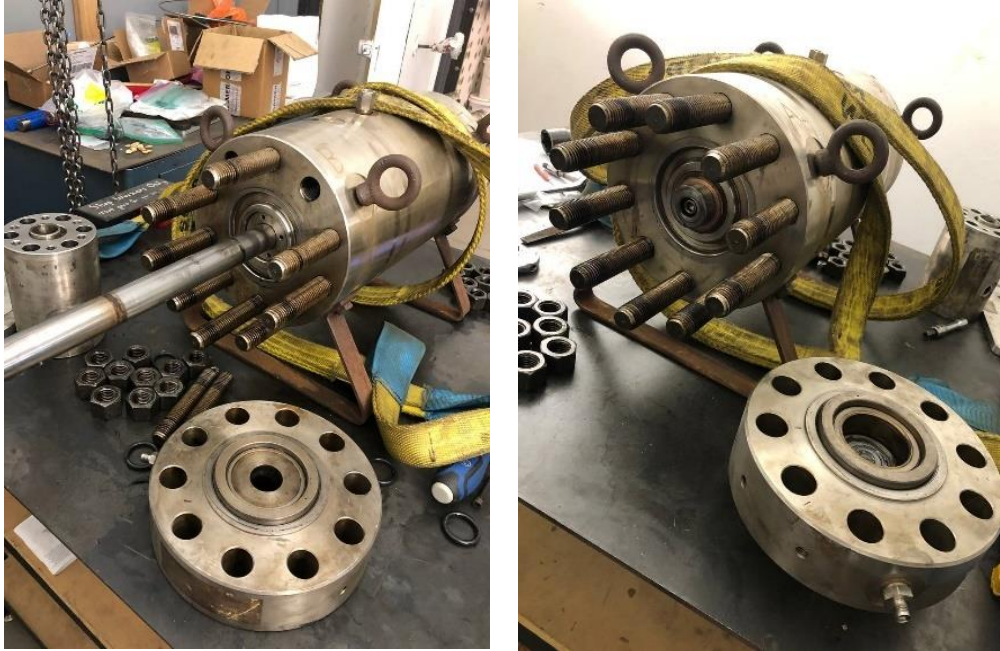
Figure 4-8: Opening endcaps

After opening the endcaps, a double o-ring described previously can be removed from the shaft. There is no barrier for the rear endcap; after opening the nuts, you can directly remove that. Now that the endcaps have been removed, the bolt can be openopenedthe end of the shaft, free the small steel size spacer, and remove the bronze spacer (Figure 4-9).
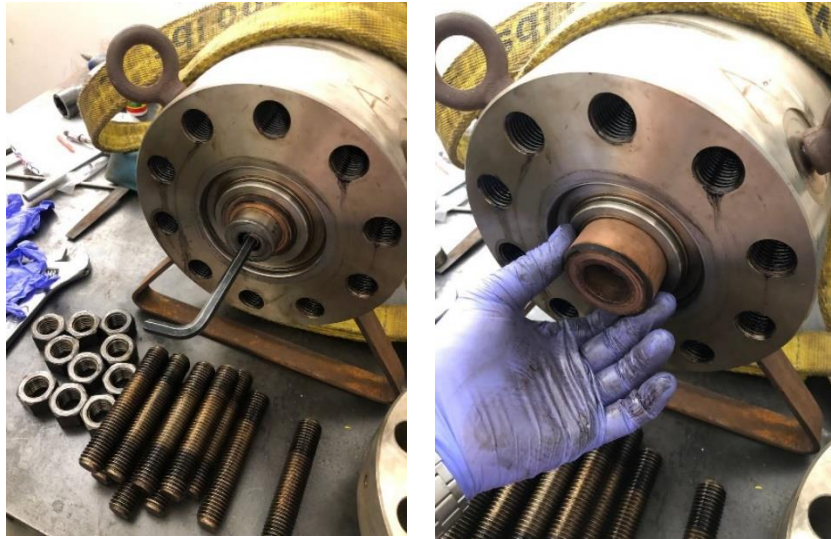
Figure 4-9: Removing outer spacers

The bronze spacer is used to hold the shaft in the center of the vessel, and it does not have any thread. Please consider that the original stainless steel spacer has been threaded. Those threads are just another part of safety that prevents the shaft from shooting out in high-pressure accumulation at the low-pressure side. In this set of experiments, the threaded spacer causes friction and unbalances the shaft since it is rotating. Now that can access the shaft, need to open the inner spacer on the front of the vessel and remove the other inner spacers and v-rings. Then put the bronze threaded shaft centralizer in its place on the front. Open the threaded part of the internal spacer on the end of the shaft and push it from the front to take the other inner spacers and the v-rings on the end of the vessel and take the shaft out (Figure 4-10).

Figure 4-10: Disassembling ahaft

4.4 Installing New Barriers

To install new seals, the centralizer should be installed on the side of the vessel that the shaft connects to the motor. Then you can pass the shaft through the centralizer, install the seals on the shaft at the end of the vessel, and assemble all spacers and threaded spacers. Now you can remove the centralizer, assemble the seals on the vessel's front side, install the interior spaces, and close the endcaps.

To install the endcaps, you should oil the nuts. After tightening the nuts, you should double-check the nuts since tightening the nuts on one side may cause displacement on another side.

In dynamic tests, you need to install a double o-ring on the front side of the vessel after installing the front endcap. Now you can put double o-rings, install the spacer, and assemble the head of the vessel to install the adapter plate.

Install the adapter plate and use a pulley system to put back the vessel and adjust its position based on the low-pressure lines. Now you have to install the u-joint without an extra push on the shaft since that extra push may cause an unbalanced position on the shaft and decentralize it.

Connect the alignment rods and pressure lines. Fix the position of the electric motor and start to check the systems.

4.5 Testing System Before Starting an Experiment

First, turn on all the corresponding electronics. Then check the lights on the DAQ device and make sure it has power. Check the connection of the DAQ device to the computer. Run the LabView program.

Open the low-pressure side A and B and the high-pressure line by clicking on the LabView program, as shown in Figure 4-11.
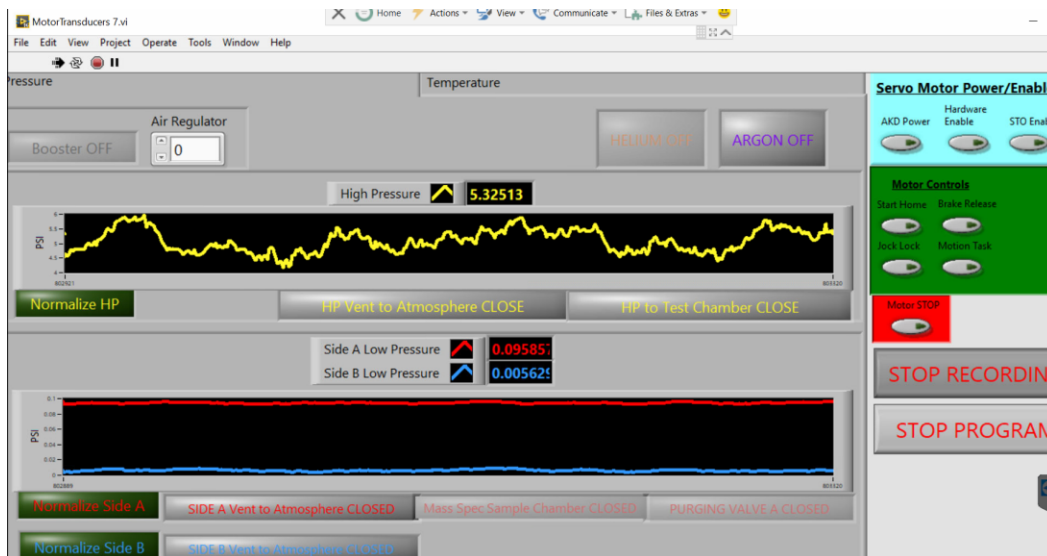
Figure 4-11: Open low-pressure and high-pressure lines to the atmosphere

Then click on the normalize to normalize the pressure to zero. Close the pressure lines vent to atmosphere and ope side A, manually inject some air into the valve, and then close it. Check the

LabView program and ensure there is no leak from the low-pressure side to the high and reverse. Do the same steps for side B, the low-pressure side.

Release the low-pressure sides and leave the vent valves open. Use bottle pressure to check the leak on the high-pressure side; if there is no leak, you can close the low-pressure sides and check if the pressure is stable.

4.6 Set Temperature

In this stage, based on the experimental requirement,s the temperature can besetd on Pthe ID controller to varietyty rangesnge. In this set of experim,ents tests have been conducted at room temperature, 121C, and 204C.

4.7 Starting Rotation

Now depressurize the system and check the rotational system. Turn on AKD Power, Hardware Enable, and STO Enable concerning Figure 4-12.

Figure 4-12: Starting motor driver in LabView

 Wait to recognize the motor driver by the second computer. Connect the motor driver to the network as shown in Figure 4-13.
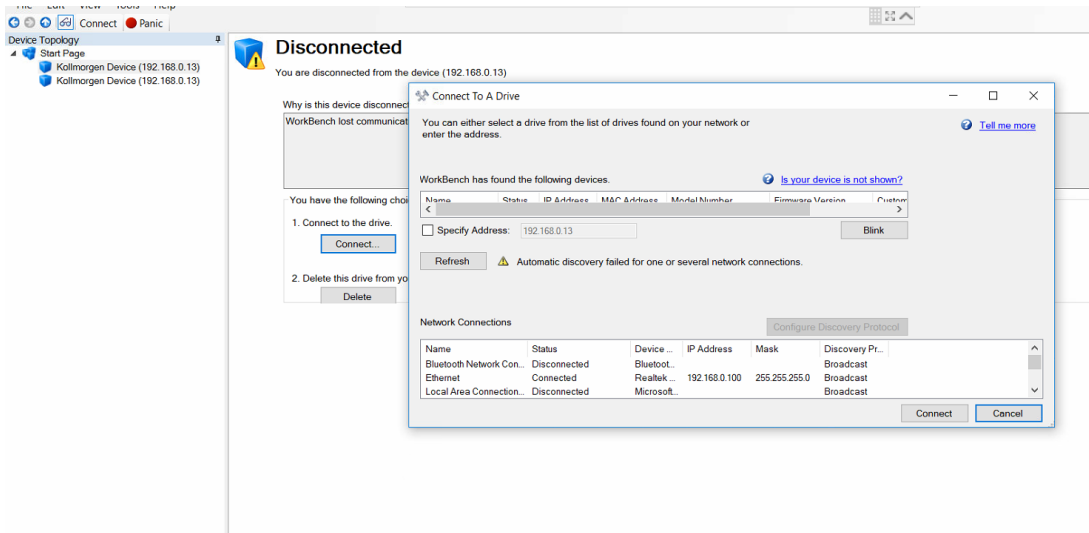
Figure 4-13: Connecting motor driver to DAQ

Enable the motor and go to the task table to program the motor motion (Figure 4-14) and (Figure 4-15).
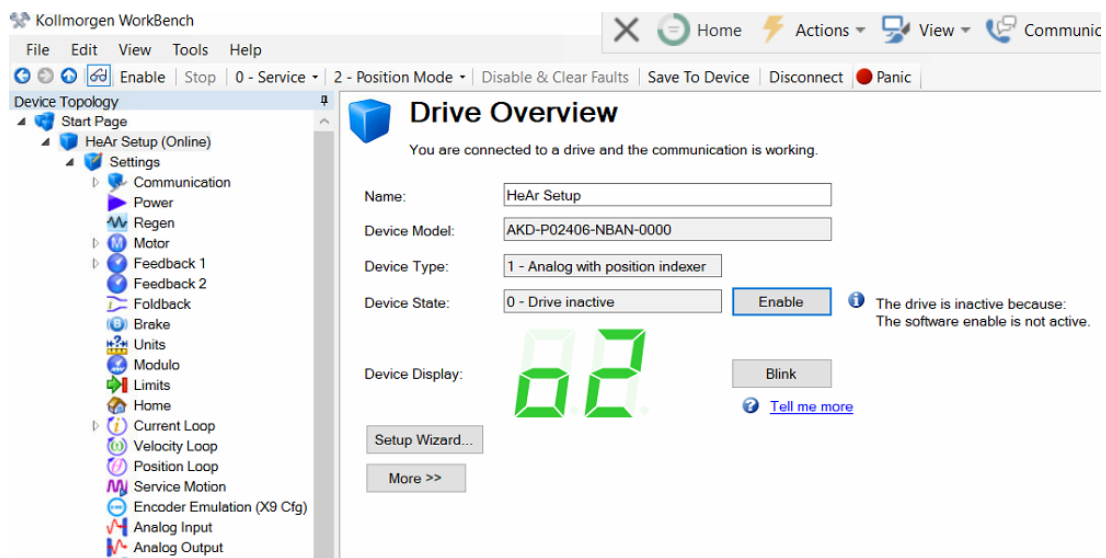
Figure 4-14: Enabling driver
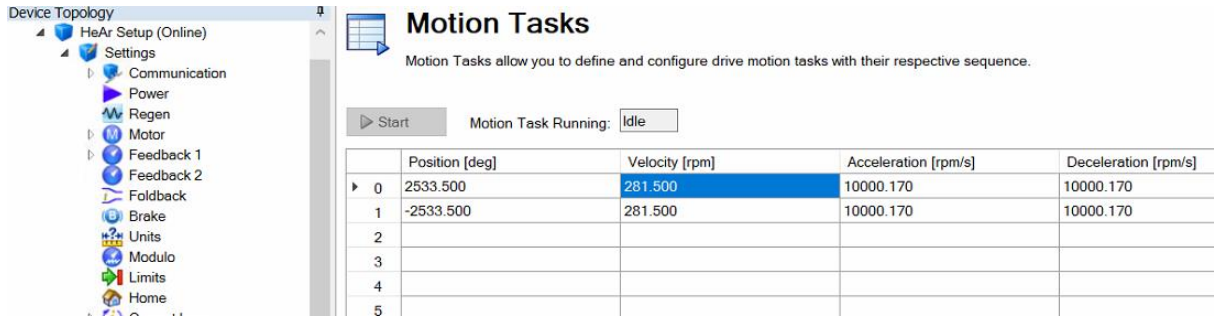
Figure 4-15: Programing task table

Save motion to the motor driver is shown in Figure 4-16. This feature will not save the motion to the device, so when you turn off the motor driver and start it over, the program will change. Here for 10 rpm, changed the velocity of the motor to 281.50 since the gear ratio is 1 to 28.15. Acceleration and Deceleration speed is 10,000.170 rpm/sec based on factory suggestion.
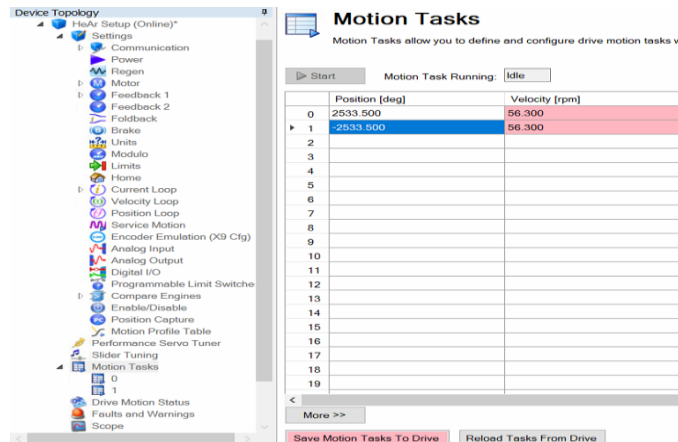
Figure 4-16: Saving motion to the driver

After saving the driver's motion task, you should turn on the Start Home to homing the shaft's position shown in Figure 4-17.

Figure 4-17: Homing the shaft position

Turn off the homing and start the motion shown in Figure 4-18.

Figure 4-18: Starting the motion

Open the low-pressure vent valves and pressurize the high-pressure side. Close the low-pressure valves. Continue to experiment until accumulated pressure in one of the low-pressure sides reaches fifteen psi.

To stop the experiment, open all valves and stop rotation. Then stop recording data. Continue to run the LabView program and monitor the low-pressure sides to depressurize the saturated gas in the barriers.

Consider that during rotational experiments, the Motor STOP should be off at all times until when want to stop the motion and turn off the Motion Task shown in Figure 4-19.

43

Figure 4-19: Stoping the rotation

4.8 Set the High-Pressure

In this study v-rings have been tested at 600, 2,250, 3,750, 6,750, and 10,000 psi. at the room temprature, 121C, and 204C. the test gas was argon, and bottle pressure was 2,500 psi. to increase the pressure on high-pressure side a gas booster was used.

4.9 Converting Data

An ideal gas law has been used to have a consistent data set and eliminate the temperature fluctuations. Based on the ideal gas law, you can change temperature fluctuations to pressure fluctuations in a constant volume. So, you can eliminate the effect of temperature fluctuations on your dataset.

4.10 Calculating Leak Rate

The accumulated pressure has been recorded to calculate the leak rate, and the slope of the pressure over time has been extracted from the data. Each experiment has been done at least three times, and the average leak rate is calculated as the output of the experiment for each condition. Figure 4-20 shows a sample of row data. Figure 4-20 shows that after accumulated pressure in low-pressure side A reaches 15 psi, the solenoid valve automatically opens to release the pressure.

44
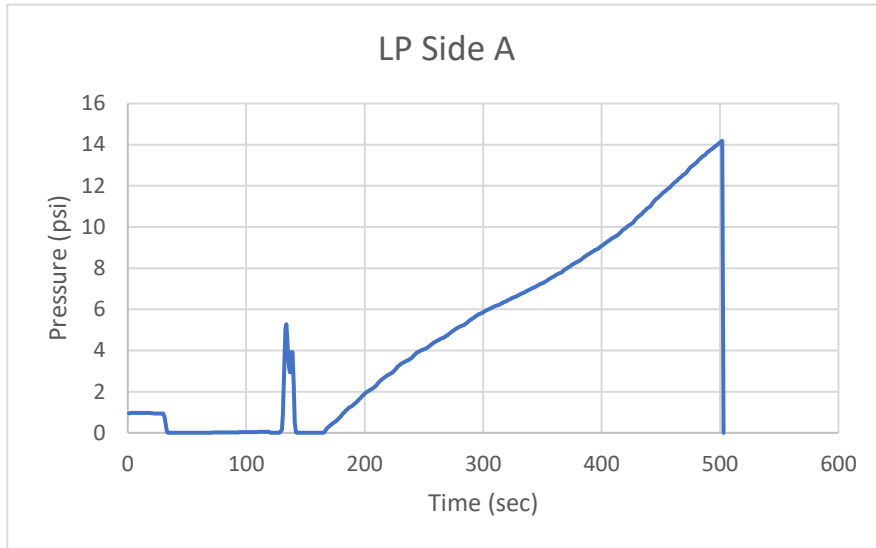
Figure 4-20: A sample of row data

4.11 Summary of Chapter Four

Chapter four discusses how to release the system, disassemble it, install new seals, and test it before starting an experiment. This chapter offers that you can use the ideal gas law to convert the data to a useable dataset. By calculating the slope of the accumulated pressure on the low-pressure side, the leak rate can be calculated.

Machine Learning Modeling

5.1 Supervised Machine Learning Methods

The mathematical model developed in this study is based on artificial neural networks, k-nearest neighbors, and support vector machines. These techniques are considered supervised modeling methods. The machine learning methods can generally be divided into supervised and unsupervised learning methods. Supervised learning involves using labeled training data to train a function that can be generalized to new samples. The training includes a critic who can provide feedback on whether or not the function is accurate and, if necessary, change the function to achieve the desired result. In supervised learning, input and the desired output are paired with labeled training data to build a function (or model). This form of supervision is expressed in the desired output, which allows you to fine-tune the function according to what it actuaces. Using further observations (predictions or classifications) following training may result in a useful output (reaction) [16].

Figure 5-1 illustrates that the supervised learning algorithm uses a labeled data set to create a model. You may then utilize this model to test the model's correctness with new data or in production with real data [17].
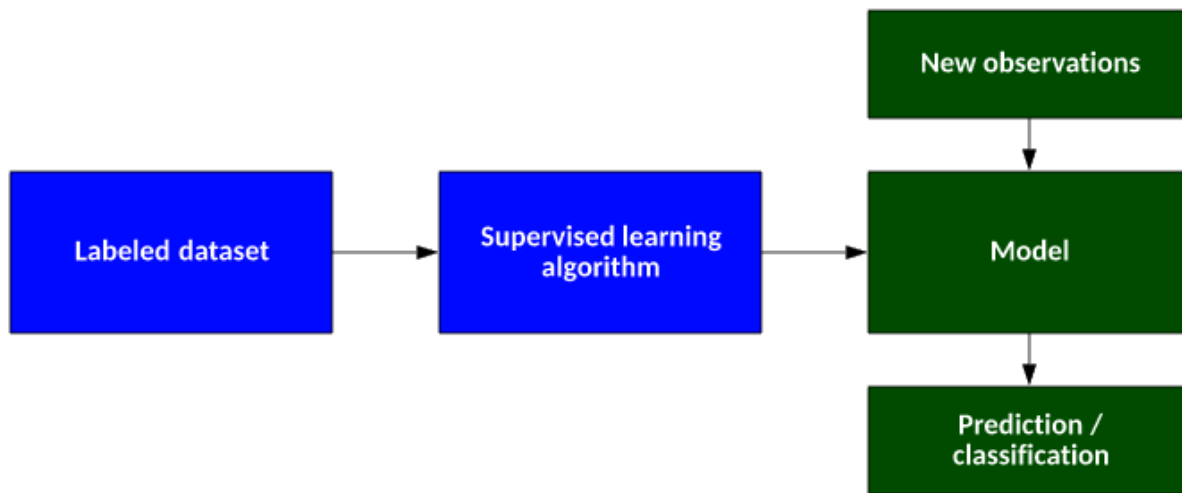
Figure 5-1: The supervised learning algorithm

5.2 Artificial Neural Network

5.2.1 Background and Literature Review

A neural network and genetic algorithm are examples of computer models used in Soft computing. On the other hand, stochastic and statistical methods are part of hard computing techniques known as NP (verifiable in nondeterministic polynomial time). Modeling and analysis with a tolerance for uncertainty, partial truth, and approximation have been used to develop "inexact" solutions to very complex problems using soft computing methods. An ANN is an artificial neural network (ANN), a subset of soft computing methods. Artificial neural networks mimic biological neurons in their behavior [18]. Among the different Artificial Neural Network architectures, the Multi-Layer Perceptrons (MLP, a model of Multilayer Feedforward Networks (MFN)), Recurrent Networks, Feedback Networks, and Kohonen Self-Organizing Maps (SOM) [19].

Applications of ANNs pose some difficulties, and these issues have inspired studies and research aimed at improving the standard methods of ANNs. Among these issues is the determination of

network structure for ANN model identification. Before implementing an MFN, it is necessary to decide the optimal number of hidden layers and nodes [18]. Network pruning must be done to reduce redundancy connections in order to increase network capacity [20]. And finally, lots of research has been done to improve the standard BP algorithm to overcome data over-fitting [21]. Researchers have developed ANN applications that have been linked to other techniques for soft computing in order to improve performance over a single technique. In many cases, combining ANNs with other techniques could produce better results than relying exclusively on ANNs. Therefore, in order to improve the ability of data interpretation and eliminate subjectivity in the operation of the training algorithm, the merged methods can be used in combination with individual ANNs [21].

5.2.2   ANN Architectures and Training Algorithms

Rosenblatt's original Perceptrons rely on single-layer feedforward networks, which can only create linearly distinct patterns. Therefore, to separate the inputs from the outputs with sufficient training, non-linear layers between the inputs and outputs can be added. MFN models are often called multi-layer perceptrons, constituting neural networks as universal approximators [22]. Figure 5-2 shows a one-layered hidden MLP network configuration. Most MLP networks are trained using the BP method. BP combines inputs based on network learning and supervised processes to provide calculated outputs based on the inputs and process inputs [22].

5.3 Multi-Layer Perceptron (MLP)
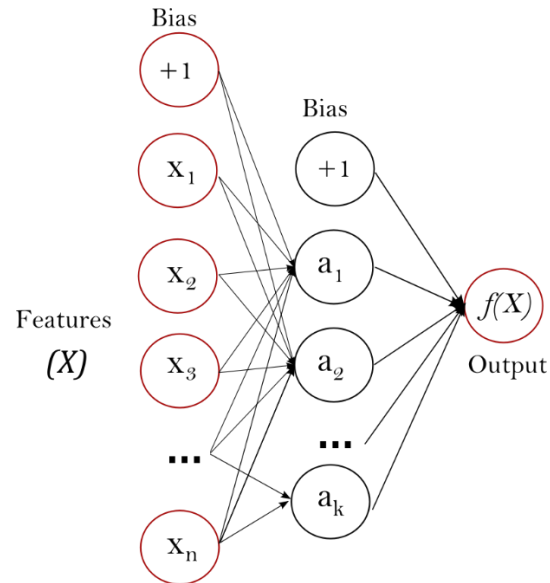
Figure 5-2: MLP data structure with one hidden layer

5.3.1 The Advantage of Multi-Layer Perceptron

To have a better understanding of the cons and pros of the Multi-Layer Perceptron followings are some advantages and disadvantages of MLP:

- It is possible to learn non-linear models.

- Possible to learn models in real-time (online learning) using partial_fit.

The disadvantages of Multi-layer Perceptron (MLP) include:

- MLP with hidden layers has a non-convex loss function where more than one local minimum exists. Therefore different random weight initializations can lead to different validation accuracy.

- MLP requires tuning several hyperparameters, such as the number of hidden neurons, layers, and iterations.

- MLP is sensitive to feature scaling [17].

To have an accurate model, one need to tune the hyperparameters of the model. One of the most used methods to tune the hyperparameters is GridsearchCV with MLPRegressor tunning method.

5.3.2 Hyperparameters for ANN

The following hyperparameters result from running code and calculation based on the GridSearchCV method shown in Figure 5-3.

```
1   # best hyperparameters_MLP
2   tuning_MLP_model.best_params_

{'activation': 'logistic',
 'alpha': 0.0001,
 'hidden_layer_sizes': (50, 100, 50),
 'learning_rate': 'constant',
 'max_iter': 2000,
 'solver': 'adam'}
```

Figure 5-3: Multi-layer perceptron hyperparameters

The architecture of the ANN is considered as follows:

Since there are three input variables, the input layer three thre nodes and hree hidden layers. Number of the nodes in hidden layers has been found by GridSearchCV method. The best combination includes 50 nodes for the first layer, 100 nodes for the second and 50 nodes for the third layer. Since there is just one out come the last layer has one node.

5.4 K-Nearest Neighbor

With the nearest neighbor method, a set of training samples is used to predict the label for a new point. User-defined sampling can be accomplished using k-nearest neighbor learning or radius-

based neighbor learning. There are many different ways to measure distances: the most common is to use the standard Euclidean distance. Neighborhood-based methods are considered non-generalizing machine learning methods since they simply "remember" all their training data (possibly transformed into a fast indexing structure such as the KD Tree or Ball Tree) [23].

Despite its simplicity, nearest neighbors effectively deal with a wide range of classification and regression problems. For instance, they effectively deal with handwritten digits and satellite images. Since it is non-parametric, it is useful when the decision boundary of a classification situation is very irregular [23].

5.4.1 K-Nearest Neighbors Regression

The neighbors-based regression method can be used when the variables are continuous instead of discrete. In order to determine the label of a query point, its closest neighbors are averaged [23].

Specifically, Scikit-learn implements two neighbor regression models: first, the regression pattern is derived from k nearest neighbors of each query point. The user specifies what k is. As a second example of learning, in the Radius Neighbors Regressor, the user specifies the radius of the neighbors in which learning takes place[23].

Advantages of KNN:

- Training time is low. There is no learning during the training phase.

- Adding new data to the KNN algorithm is seamless because the algorithm requires no training prior to making predictions.

- Implementation of the KNN algorithm is straightforward. KNN can only be implemented with two parameters, namely K and the distance function [24].

Disadvantages of KNN:

51

- Algorithm does not perform well for large datasets: large datasets impose a high cost on calculating the distances between new points and existing points, resulting in poor performance.

- A KNN algorithm does not work well with high dimensions because it becomes difficult for the algorithm to calculate distances among dimensions with a large number of dimensions.

- Before applying the KNN algorithm to any dataset, needs to perform feature scaling (standardization and normalization). If don't do this, KNN may generate incorrect predictions.

- Sensitive to missing values, outliers, and noisy data: KNN has a sensitivity to data that contains noise. Incomplete data must be imputed manually, and outliers must be removed [24].

5.4.2 KNN Hyperparameters

To find the best hyperparameters here, a GridSearchCV method with five-folds has been used, and the results have been compared with metrics for regression problems.

```
1   # best hyperparameters_KNN
2   tuning_KNN_model.best_params_

{'n_neighbors': 2, 'weights': 'uniform'}
```

Figure 5-4: KNN hyperparameters

5.5 Support Vector Machine Regression

Support Vector Machines (SVM) are among the most known and widely used algorithms for classification problems in machine learning. Also, can use them in solving regression problems.

The SVM regression algorithm is known as Support Vector Regression or SVR. Support Vector Machines are supervised learning models. Supervised learning models are the machine learning task of learning a function that maps an input to an output. SVR is associated with learning algorithms that analyze data used for regression analysis in machine learning[25].

In SVM, the straight line required to fit the data is called a hyperplane. This method searches for a hyperplane in multi-dimensional space [26]. This hyperplane can classify the data points. The closest data points on any side of the hyperplane are called Support Vectors [26]. These support vectors influence the position and orientation of the hyperplane and help to build the SVM [26]. The Support Vector Regression (SVR) uses the same principle as the SVMs. Generally, the idea behind SVR is to find the best fitting line. In the SVR, the best fit line is the hyperplane with the maximum number of points. SVR fits the best line considering a threshold value. The threshold value is the distance between the hyperplane and the boundary line. The complexity of SVR is more than quadratic with the number of samples. So, it is hard to scale to datasets with more than a couple of 10,000 samples, and that is why SVR is suitable for a low number of data points [25].

Support vector regression (SVR) can be used to solve both linear and non-linear models [27].

Advantages:

- SVR has a computational complexity, and it does not depend on the dimensionality of the input space.
- SVR has excellent generalization capability with high prediction accuracy [28].

Disadvantages:

- Not suitable for large datasets

- If the number of features for each data point were more than the number of training data samples, the SVM would underperform.

- It has not performed well when the data set has more noise [25].

5.5.1 Hyperparameters in SVR

The followings are the hyperparameters for SVR generated by the GridSearchCV method:

```
# best hyperparameters_SVR
svr_tuning_model.best_params_
{'C': 0.01, 'epsilon': 0.01, 'gamma': 0.01, 'kernel': 'linear'}
```

Figure 5-5: Best hyperparameters for SVR

5.6 Overview of the Data

Table 5-1 gives us a general view of the data. Here can see the data set has four attributes. In Table 5-1, pressure, temperature, and rotational speed, respectively, have been shown by psi, temp, and rpm. The ratio represents the average leak rate. In this set of experiments, each experiment has been repeated at least three times to have a scientific point of view on the phenomena to calculate the average leak rate. This set of experiments could generate 45 experimental data points. The results of the experiments with no leak or unusual leak have been eliminated and have not been considered.

Table 5-1: An overview of the data

	psi	temp	rpm	ratio
0	600	20	0	0.001000
1	2250	20	0	0.012967
2	3750	20	0	0.013600
3	6750	20	0	0.033800
4	10000	20	0	0.316050

Table 5-2 ratio represents the accumulated leak rate pre-second.

5.7 Outliers

First, need to find the outliers to start the data analysis. Here to find the outliers, a box plot has been used. Using a Z score method and considering a threshold equal to 3, could generate a box plot shown in Figure 5-6
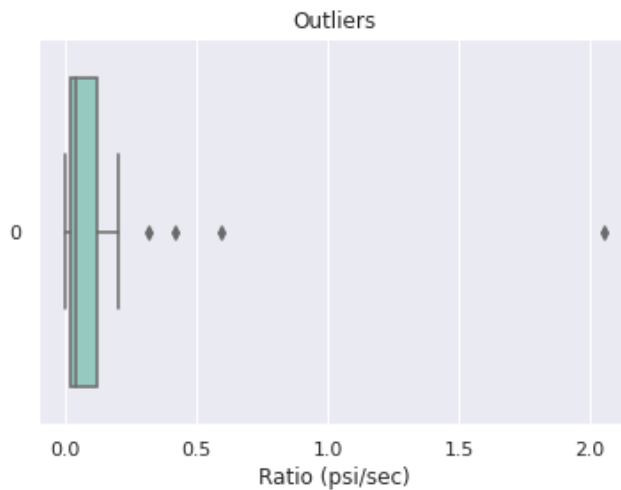

Figure 5-6: Outliers

Z-score is a numerical measurement method that describes a value's relationship to the mean of a group of data. Z-score is measured in terms of standard deviations from the mean. A Z-score with a threshold equal to 3 means a value that is three standard deviations away from the mean [29].

Figure 5-6 suggests that if there is an outlier, it will be plotted as a point in the boxplot, but other populations will be grouped together and displayed as boxes. From **Error! Reference source not f ound.**, four data points in outliers, and after dropping these data points, mode uses 41data points. 75 percent of the data randomly used to run the modeling. Here a GridSearchCV method has been used for all three modelings and applied the data folding method with five folds. So, in each fold, the data has been divided into five sets and then used four of them for training and the fifth one for the test to calculate the error. Results are shown in Table 5-2.

5.7.1   Errors of Each Method

Table 5-2: Error for each method

Method	Mean Squared Error
MLP	0.0904
KNN	0.6800
SVR	0.084

Table 5-2 shows the error for each method. Here 75% of data has been used for training, and 25% has been used for testing. A support vector machine has been used in this study to model the data based on error calculations.

5.8 Summary of Chapter Five

This chapter introduces Multi-layer Perceptron as an artificial neural network method, k-nearest neighbor, and support vector machine. All these methods are supervised methods means the input

data has been labeled and has a test data set to measure the accuracy of the methods. Here Python has been used as a programing language, and hyperparameters have been calculated by the GridSearchCV method. To have an accurate error number of the fold was five, and sampling was random. MLP has the lowest error and could generate a better model based on calculations.

Chapter Six: Results and Conclusion

The input data is expressed in Table 6-1 data matrix in this study. In this study, the emission tests with argon as a test gas on v-ring barriers have been coducted. In this set of experiments, have generated data for room temperature, 121C, and 204C. The pressure range was 600, 2250, 3750, 6750, and 10,000 psi. Considering that these seals are used on applications with rotation, all experiments have been conducted in static, 2 rpm, and 10 rpm shaft speeds. Results have been saved as accumulated pressure on the low-pressure side, and the experiment was stopped when the accumulated pressure on the low-pressure side was 15 psi. The data was recorded every second. Each experiment has been repeated at least three times, and the pressure (psi) increases slope based on the time (second) was converted considering the temperature in celsius. The final data shows the average leak rate of argon in different conditions.

Table 6-1: Data matrix

	Static	Static	Static	2rpm	2rpm	2rpm	10rpm	10rpm	10rpm
600psi	25C	12C	204C	25C	12C	204C	25C	12C	204C
2250psi	25C	121C	204C	25C	121C	204C	25C	121C	204C
3750psi	25C	121C	204C	25C	121C	204C	25C	121C	204C
6750psi	25C	121C	204C	25C	121C	204C	25C	121C	204C
10ksi	25C	121C	204C	25C	121C	204C	25C	121C	204C

V-rings for dynamic and static tests in this set of experiments have been used. These tests contain rotating motion applications, and seals create a barrier between fixed or moving surfaces. These

seals are used to separate or hold fluids, pressure, and pollutants. Table 6-2 shows the list of the v-rings that have been used.

Table 6-2: Seals configurations

Config. #	Seal 1	Seal 2	Seal 3	Seal 4	Seal 5	Retainer R	Adapter A	Schematics
E	T1	T1	T1	F1	F1	R-1	A-1	

We have started the tests with a configuration of Seals 1, 2, and 3 and then moved to configuration E includes seals 1, 2, 3, 4, and 5. In both configurations, v-rings are surrounded by spacers at both ends. Configuration E includes three T1 v-rings and two F1 v-ring in the head where the high-pressure test gas was introduced. The configurations of the three seals were not holding any pressure at room temperature. So, configuration E with five layers of v-rings has been used. This configuration could hold the gas pressure at 10,000, 6750, 3750, 2250, and 600 for room temperature, 121C, and 204C. Figure 6-1 shows the v-rings packing in configuration E. Also, the spacers on both sides of the v-rings are shown.

Figure 6-1: V-ring config

Since the test setup is symmetric, the same configuration of seals was used on both sides of the test vessel. The pressure leak has been calculated by measuring the accumulated pressure on the low-pressure side.
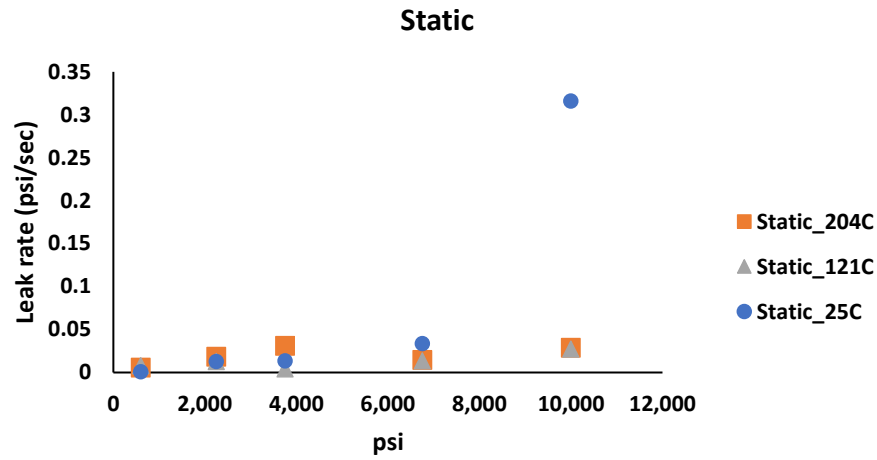
6.1 Experimental Data

Figure 6-2: Leak rate in different pressures and static shaft

Error! Reference source not found. shows by increasing temperature, leak rates have been raised a

t all pressures. Also, by increasing pressure leak rate is increasing in static tests. This figure shows

that the temperature significantly affects the leak rate when have higher pressure.
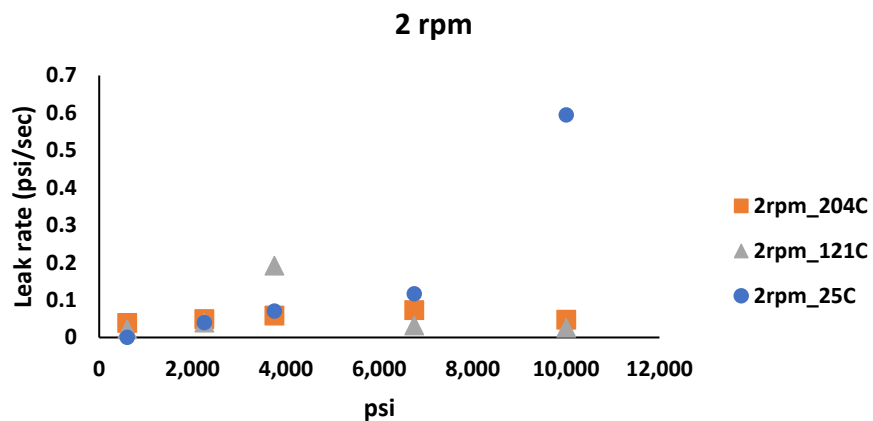

Figure 6-3: Leak rate in different pressures for 2 rpm

Figure 6-3 shows the leak rate for 2 rpm at different pressures, indicating that the leak rate will increase by increasing pressure.
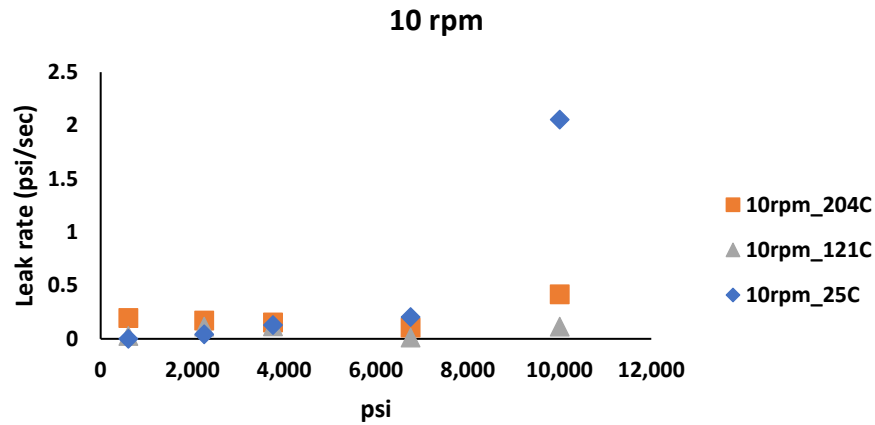

Figure 6-4: Leak rate in different pressures for 10 rpm

Error! Reference source not found. shows the experimental data on a rotating shaft with 10 rpm s peed. This figure indicates that the effect of the pressure is more than the effect of the temperature.

6.2 Support Vector Machine Regression (SVR) Modeling Results

This study used an artificial neural network, k-nearest neighbor, and a support vector machine regression (SVR) to model the experimental data. Error analysis shows that the SVR could generate a model with the lowest error. Results are shown in figures 6-5, 6-6, 6-7, respectively, for static, 2 rpm, and 10 rpm data.
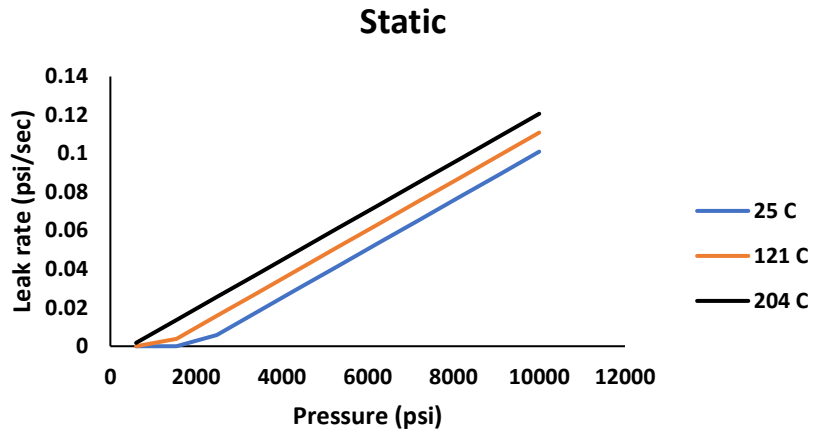
Figure 6-5: Machine learning modeling results for static shaft

Figure 6-5 shows the SVR modeling results for the static shaft. When the test gas pressure is lower than 2000 psi in all temperatures, the model predicts that the leak rate is almost zero or close to zero. For 25 C and 121C in the static shaft, increasing the pressure from zero to more than 2000 psi model predicts a curve, and then it gets almost a constant slope for higher pressure. In 204 C, the model predicts almost a constant slope for all pressures.

Figure 6-6: Machine learning modeling results for rotating shaft with 2 rpm

Figure 6-6 indicates that even in 600 psi model predicted a leak rate. Experiencing an almost constant slope in leak rate for all temperatures. Also, with increasing the temperature leak rate slope has been increased.
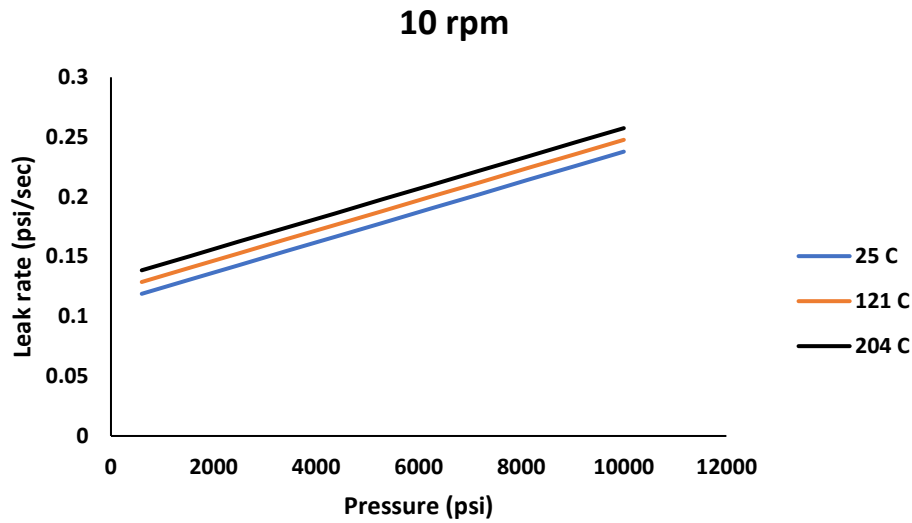
10 rpm

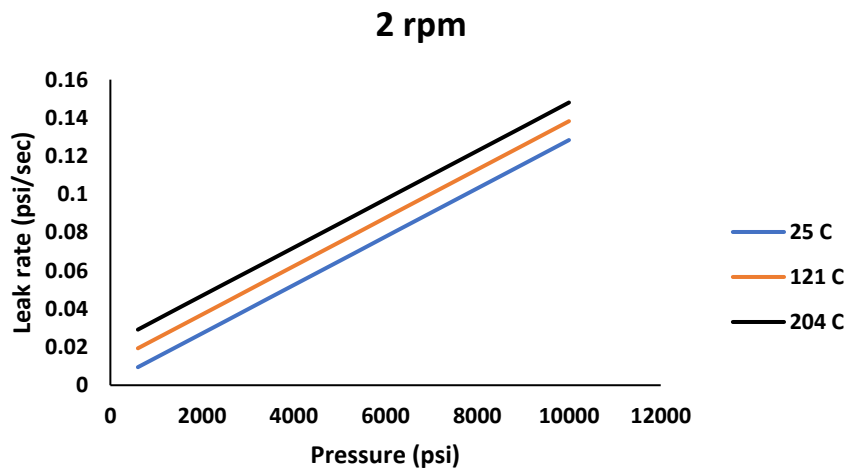

Figure 6-7: Machine learning modeling results for rotating shaft with 10 rpm

Figure 6-7 shows the SVR modeling leak rate results for a shaft that rotates at 10 rpm. Since the rotation speed of the shaft has a significant effect on the leak rate, the predicted leak rate lines are very close and include a higher magnitude comparing the 2 rpm rotational speed and static shaft. SVR modeling results show that at 10 rpm rotational speed, the leak rate slope is almost constant from the beginning of the graph. This indicates a high leak even at low pressure. Figure 6-7 shows that in 10 rpm rotational speed, the temperature can also impact the leak rate for any pressure.
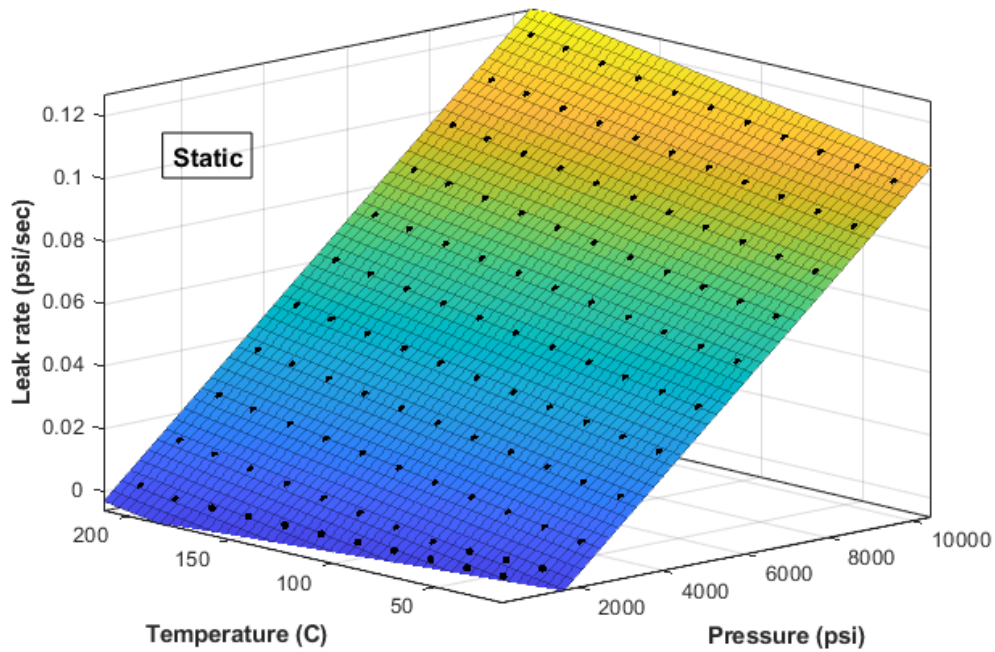
Figure 6-8: SVR modeling results for a static shaft in 25C to 204C temperature range and 600 psi to 10,000 psi pressure range

Figure 6-8 shows an overview of various temperatures and pressures on the static shaft generated by SVR. 121C data points have been used on a static shaft to generate the surface plot. These data points contain a temperature range between 25C to 204 C and a pressure range between 600 psi and 10,000 psi. Figure 6-8 shows that there is an increasing slope for pressure and temperature simultaneously.

Figure 6-9: SVR modeling results for a shaft with 2 rpm rotational speed in 0C to 204C temperature range and 600 psi to 10,000 psi pressure range

Same as Figure 6-8 to generate a graph for shaft with 2 rpm rotational speed, 121 data point has been generated with SVR modeling and results for 25C to 204C, and a pressure range of 600 psi to 10,000 psi is shown in Figure 6-9. Figure 6-9 shows that in higher temperatures, leak rates are much more significant than static shaft leak rates. Also, this figure indicates that the leak rate slope generally is higher than the static shaft.
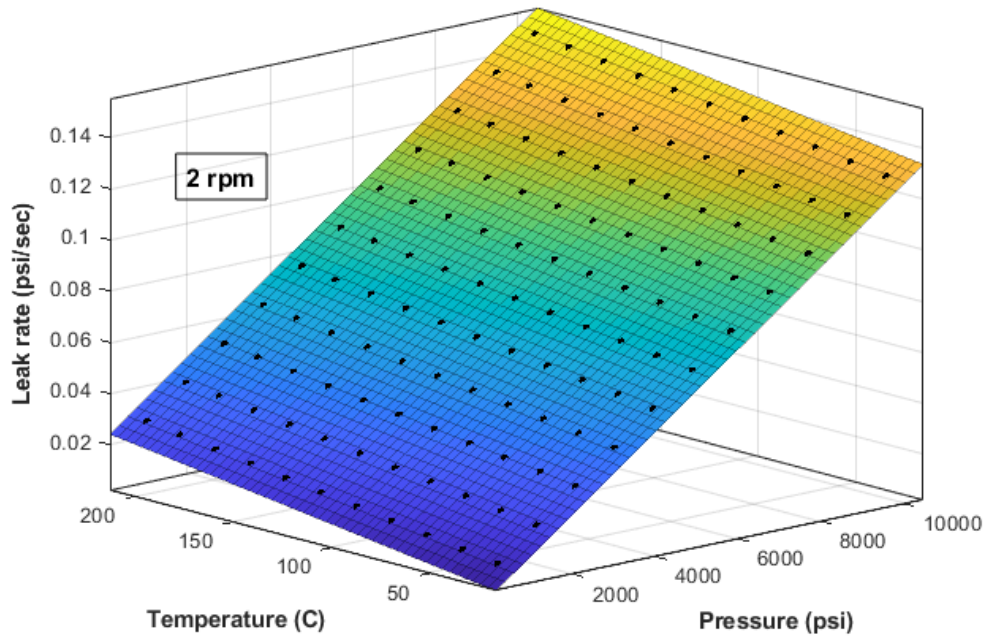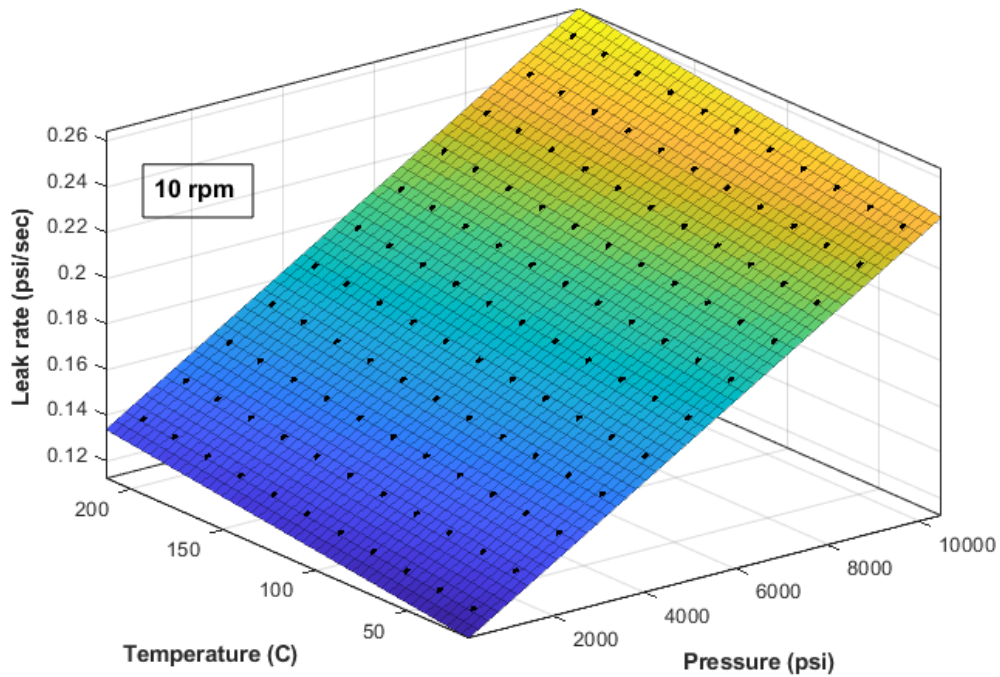
Figure 6-10: SVR modeling results for a shaft with 10 rpm rotational speed in 0C to 204C temperature range and 600 psi to 10,000 psi pressure range

To generate Figure 6-10 eleven points for temperature and eleven points for pressure in constant rotational speed for the shaft have been used. All 121 data points have been generated through SVR modeling. Figure 6-10 shows that the leak rate slope is much higher than 2 rpm and static shaft with increasing pressure and temperature.

$$f(x, y) = a + bx + cy + dx^2 + exy + fy^2$$ Equation 1

Equation 1 shows the general equation resulting from SVR modeling, and its coefficients are shown in Table 6-3. Here, x represents pressure, and y represents temperature.

Table 6-3: Equation coefficients resulting from SVR modeling

	Coefficients (with 95% confidence bounds):	
Static Shaft	a = -0.02824 b = 1.265e-05 c = 0.0001098 d = 2.802e-18 e = 1.97e-16 f = -1.158e-14	R-square: 0.9993 Adjusted R-square: 0.9993 RMSE: 0.0009938
2 rpm	Coefficients (with 95% confidence bounds): a = -0.000876 b = 1.265e-05 c = 0.0001098 d = 5.516e-18 e = -1.613e-16 f = -2.26e-15	R-square: 1 Adjusted R-square: 1 RMSE: 3.099e-10
10 rpm	Coefficients (with 95% confidence bounds): a = 0.1086 b = 1.265e-05 c = 0.0001098 d = 1.319e-18 e = -1.374e-17 f = -3.607e-15	R-square: 1 Adjusted R-square: 1 RMSE: 3.377e-10

6.3 Conclusion

In this study, a set of experimental data have been generated from a high-pressure test setup. The test setup includes pressure and temperature indicators and controllers to run tests in a temperature range of -46 C to 204 C and a pressure range of bottle pressure to 10,000 psi. The test setup has been equipped with an electric motor and motor driver to control the rotation of the shaft. For this research, emissions of argon over a set of v-rings with static, 2 rpm, and 10 rpm rotational speeds of a shaft have been measured at 25C, 121C, and 204C and in 600, 2250, 3750, 6750, and 10,000 psi. The experimental data have been used to generate machine learning models. Artificial neural networks, k-nearest neighbor, and support vector machine regression have been used to model the experimental data. Error analysis shows support vector machine regression could be the ultimate modeling method with the experimental data set. Using the support vector machine regression

method, a new set of data has been generated, and based on that, an equation for constant rotational speed has been generated. The surface pane graph in figures 6-8, 6-9, and 6-10 have been generated using this equation. The coefficients and fitting error for the static shaft and the shaft with 2 rpm and 10 rpm rotational speed have been presented in tables 6-3. Results show the impact of temperature and rotational shaft's speed in laek rate is significant. Results of this study are applicable on valve, comprassore and any type of dynamic seal test process. Generally, the applications of this study can be on reducing the cost of the production and leak rate tests in rotational equipment design for oil and gas industry.

6.4 Future works

To find a correlation, future tests could be performed with helium, Carbon Dioxide, and methane.

Another application for the setup would be to test spring-energized seals with multiple layers.

As the setup has a cooling chamber, the experiments can be repeated at lower temperatures in the future.

References

[1]   K. Sotoodeh, "Why packing adjustment cannot stop leakage: Case study of a ball valve failing to seal after packing adjustment during fugitive emission as per ISO 15848–1," *Eng. Fail. Anal.*, vol. 130, 2021, doi: 10.1016/j.engfailanal.2021.105751.

[2]   J. Penman, M. Gytarsky, T. Hiraishi, W. Irving, and T. Krug, *2006 IPCC - Guidelines for National Greenhouse Gas Inventories*. 2006.

[3]   M. KAZEMINIA and A.-H. BOUZID, "Prediction of gas flow in compressible and low permeability porous media," *J. Fluid Sci. Technol.*, vol. 10, no. 2, pp. JFST0018–JFST0018, 2015, doi: 10.1299/jfst.2015jfst0018.

[4]   "ISO 15848-1 ," *INTERNATIONAL STANDARD*, May 01, 2015. http://www.pacificcrn.com/Upload/file/201702/16/20170216135006_90356.pdf (accessed Apr. 07, 2022).

[5]   S. Raman, Z. Siddique, K. Barker, P. Huebner, and R. Madhavan, "Predictive Modeling in Fugitive Emissions Testing," 2020, Accessed: Apr. 07, 2022. [Online]. Available: https://shareok.org/handle/11244/325365.

[6]   Leak Testing & Pressure Testing: Guide to Helium Leak Testing | TQC. (accessed Apr. 07, 2022).

[7]   E. Weidner, M. Honselaar, R. JRC, and B. Gindroz, "CEN-CENELEC," 2016, doi: 10.2790/66386.

[8]   M. Bram *et al.*, "Deformation behavior and leakage tests of alternate sealing materials for SOFC stacks," *J. Power Sources*, vol. 138, no. 1–2, pp. 111–119, Nov. 2004, doi:

10.1016/J.JPOWSOUR.2004.06.041.

[9]   Y. Lim and R. M. Ismail, "The shortage of helium supply in industry," 2013, Accessed:

Apr. 08, 2022. [Online]. Available: https://repo.uum.edu.my/id/eprint/11705/.

[10]   S. A. Stern *et al.*, "The Discovery of Argon in Comet C/1995 O1 (Hale-Bopp),"

Astrophys. J., vol. 544, no. 2, pp. L169–L172, Dec. 2000, doi: 10.1086/317312/META.

[11]   "AN Style V-Rings, Aflas® Seals & Viton® Seals | Precision Associates Inc."

https://catalog.precisionassoc.com/viewitems/product-catalog/v-

rings?bc=100%7C1017%7C1013 (accessed Apr. 07, 2022).

[12]   "Thermocouple-Thermocouples-What is a thermocouple-Types of thermocouples."

http://www.thermocoupleinfo.com/ (accessed Apr. 07, 2022).

[13]   "How Do PID Controllers Work | PID Working Principle." https://www.omega.com/en-

us/resources/how-does-a-pid-controller-work (accessed Apr. 07, 2022).

[14]   "USB-6353 National Instruments Multifunction I/O Device | Apex Waves."

https://www.apexwaves.com/modular-systems/national-instruments/x-series/USB-6353

(accessed Apr. 08, 2022).

[15]   "Gas Boosters & Systems Single Acting-single Stage Double Acting-single Stage Double

Acting-single Stage-two Air Heads Double Acting-two Stage-two Air Heads Double

Acting-two Stage Triple Air Head Rebreather Oxygen Boosters Gas Bottle Mounted

Charging Systems Maxpro Custom Designed Air Driven."

[16]   "What is Supervised Learning?"

https://www.techtarget.com/searchenterpriseai/definition/supervised-learning (accessed

Apr. 09, 2022).

[17] "Supervised learning models - IBM Developer." https://developer.ibm.com/articles/cc-supervised-learning-models/ (accessed Apr. 09, 2022).

[18] Y. Huang, "Advances in Artificial Neural Networks – Methodological Development and Application," *Algorithms 2009, Vol. 2, Pages 973-1007*, vol. 2, no. 3, pp. 973–1007, Aug. 2009, doi: 10.3390/ALGOR2030973.

[19] D. E. Rumelhart, G. E. Hinton, and R. J. Williams, "Learning Internal Representations by Error Propagation," *Readings Cogn. Sci. A Perspect. from Psychol. Artif. Intell.*, pp. 399–421, Oct. 2013, doi: 10.1016/B978-1-4832-1446-7.50035-2.

[20] J. Sietsma and R. J. F. Dow, "Neural net pruning - why and how," pp. 325–333, 1988, doi: 10.1109/ICNN.1988.23864.

[21] Wang, J.H.; Jiang, J.H.; Yu, R.Q. Robust back propagation algorithm as a chemometric tool to prevent the overfitting to outliers. Chemom. Intell. Lab. Syst. 1996, 34, 109-115 - (accessed Apr. 09, 2022).

[22] G. Cybenko, "Approximation by superpositions of a sigmoidal function," *Math. Control. Signals Syst. 1989 24*, vol. 2, no. 4, pp. 303–314, Dec. 1989, doi: 10.1007/BF02551274.

[23] 1.6. Nearest Neighbors — scikit-learn 1.0.2 documentation. (accessed Apr. 09, 2022).

[24] N. Kumar, "The Professionals Point: Advantages and Disadvantages of KNN Algorithm in Machine Learning," *The Professionals Point*, 2019. (accessed Apr. 09, 2022).

[25] A. Raj, "Unlocking the True Power of Support Vector Regression," *Towards Data Science*, 2020. https://towardsdatascience.com/unlocking-the-true-power-of-support-

vector-regression-847fd123a4a0 (accessed Oct. 03, 2020).

[26] "Support Vector Machine — Introduction to Machine Learning Algorithms | by Rohith
Gandhi | Towards Data Science." https://towardsdatascience.com/support-vector-machine-
introduction-to-machine-learning-algorithms-934a444fca47 (accessed Apr. 11, 2022).

[27] "Fundamental Types of Regression Analysis on Various Research Data using R
Programming | CENTRAL ASIAN JOURNAL OF MATHEMATICAL THEORY AND
COMPUTER SCIENCES."
https://cajmtcs.centralasianstudies.org/index.php/CAJMTCS/article/view/1 (accessed Apr.
09, 2022).

[28] M. Awad and R. Khanna, "Support Vector Regression," in *Efficient Learning Machines*,
Berkeley, CA: Apress, 2015, pp. 67–80.

[29] Z-Score Definition: How to Calculate Z-Score.
https://www.investopedia.com/terms/z/zscore.asp (accessed Apr. 12, 2022).